REPORT DOCUMENTATION PAGE	Form Approved OMB No. 0704-0188

1. AGENCY USE ONLY *(Leave blank)*	2. REPORT DATE	3. REPORT TYPE AND DATES COVERED
	9 Jan 97	

4. TITLE AND SUBTITLE
Fabrication of Reticulated Graphitic Foam

5. FUNDING NUMBERS

6. AUTHOR(S)
Heather J. Anderson

7. PERFORMING ORGANIZATION NAME(S) AND ADDRESS(ES)
Clarkson University

8. PERFORMING ORGANIZATION REPORT NUMBER
96-120

9. SPONSORING/MONITORING AGENCY NAME(S) AND ADDRESS(ES)
DEPARTMENT OF THE AIR FORCE
AFIT/CI
2950 P STREET
WPAFB OH 45433-7765

10. SPONSORING/MONITORING AGENCY REPORT NUMBER

11. SUPPLEMENTARY NOTES

12a. DISTRIBUTION AVAILABILITY STATEMENT
Unlimited

12b. DISTRIBUTION CODE

13. ABSTRACT *(Maximum 200 words)*

14. SUBJECT TERMS	15. NUMBER OF PAGES
	75
	16. PRICE CODE

17. SECURITY CLASSIFICATION OF REPORT	18. SECURITY CLASSIFICATION OF THIS PAGE	19. SECURITY CLASSIFICATION OF ABSTRACT	20. LIMITATION OF ABSTRACT

DISCLAIMER NOTICE

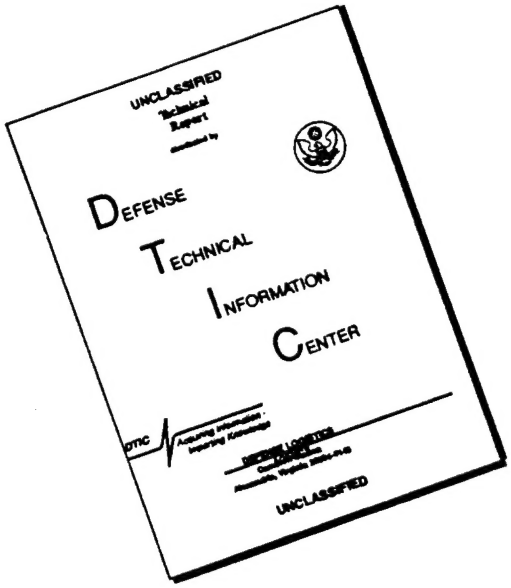

THIS DOCUMENT IS BEST QUALITY AVAILABLE. THE COPY FURNISHED TO DTIC CONTAINED A SIGNIFICANT NUMBER OF PAGES WHICH DO NOT REPRODUCE LEGIBLY.

CLARKSON UNIVERSITY

Fabrication of Reticulated Graphitic Foam

A Thesis

by

Heather J. Anderson

Department of Mechanical and Aeronautical Engineering

Submitted in partial fulfillment of the requirements

for the degree of Master of Science
(Mechanical Engineering)

August 1996

Accepted by the Graduate School

_____

Date Dean

The undersigned have examined the thesis/dissertation entitled "Fabrication of Reticulated Graphitic Foam" presented by Heather J. Anderson, a candidate for the degree of Master of Science and hereby certify that it is worthy of acceptance.

30 Aug 96
Date

Advisor - Steven W. Yurgartis

Professor - David J. Morrison

Professor - Don H. Rasmussen

ABSTRACT

Carbon foams have applications where light weight and high temperature resistant materials are required. A 3D morphology can be obtained, forming an intricate network of interconnecting struts. These struts have the potential to simulate graphitic carbon fibers with a high specific strength, high specific stiffness, high thermal conductivity, and extreme high temperature stability. Potential applications of carbon foams include: fugitive phase for inverse metal foams, rapid thermal capacitors, catalyst substrates, 3D composite reinforcement, and caustic and biological filters.

Carbon foams have been produced using blowing agents such as carbon dioxide and nitrogen, however these foams contain closed cells and have a microcellular morphology. The goal of the present work is to produce a graphitic carbon foam with open cells on the order of 10 to 18 ppi (pores per inch). A technique has been developed using polyurethane foam as a fugitive phase. The polyurethane foam is dipped into a solution of mesophase pitch (MP). Mesophase pitch is a carbon precursor, in the present case, derived from naphthalene. The advantage of MP is that it is easily graphitized. The flow of the MP over the struts gives some initial molecular orientation. The dipped foam is dried, leaving behind a the polyurethane foam coated with the pitch. The foam then goes through several heat treatments to stabilize the mesophase pitch, burn out the polyurethane, carbonize and finally graphitize the foam, all the while maintaining the same morphology as the initial polyurethane foam.

ACKNOWLEDGMENTS

I'd like to thank Dr. David Morrison and Dr. Don Rasmussen for reviewing my work. Special thanks to Dr. Rasmussen for his guidance and lengthy discussions so critical for this research. Thank you to Dr. Campbell and his graduate students for their advice and equipment. A special thank you to Rich for his time and help with the x-ray diffraction analysis. I'd like to especially thank Dr. Steven W. Yurgartis for his support. His unique leadership has provide an environment for growth.

The Material Lab members are wonderful people and great friends. Their advice and support are unmatched.

Thank you to Mitsubishi Gas Chemical Co. Inc. for supplying the mesophase pitch used in this research.

Thank you to the Air Force for giving me the opportunity to expand my education. Especially the Air Force Institute of Technology for granting me the scholarship to continue my education at Clarkson University.

My work would not have been a success without the love, faith and support of my family. I am truly grateful to them for all they have done for me. Thank you dad and John for being my strength and support. I'd like to thank my mom for inspiring me to be the best and to keep reaching for the stars. Her death was indescribably difficult.

- for Mom -

Dad and John

TABLE OF CONTENTS

1. ORGANIZATION AND BACKGROUND 1

1.1 Introduction 2
1.1.1 Applications Of Carbon Foams 2

1.2 Carbon Foams 4
1.2.1 Manufacturing Carbon Foams 5
1.2.1.1 Blowing Agent 5
1.2.1.2 Thermally Induced Phase Separation 7
1.2.1.3 Polymer Conversion 8
1.2.1.4 Mesophase Pitch Coated Polyurethane Foam 9
1.2.1.5 Substrate Replication Process 9

2. CARBON FIBERS AND PRECURSORS 11

2.1 Carbon Fiber Manufacturing 11

2.2 Precursors 12
2.2.1 Polyacrylonitrile 12
2.2.2 Pitch 13
2.2.2.1 Mesophase Formation 15

3. PRODUCTION OF CARBON FOAMS WITH A BLOWING AGENT 17

3.1 Direct Blowing 17
3.1.1 Process 18
3.1.2 Gas Saturation 19
3.1.3 Bubble Nucleation 26
3.1.4 Bubble Growth 28
3.1.5 Results 31

3.2 Reblowing 33
3.2.1 Process 33
3.2.2 Results 34

3.3 Conclusions 35

4. COATED POLYURETHANE FOAM 36

4.1 Process 36
4.1.1 Coating 37
4.1.2 Heat Treatment 37

4.2 Results 38
4.2.1 X-Ray Diffraction 48
4.2.2 Scanning Electron Microscopy 62

4.3 Conclusions And Future Work 69

5. SUMMARY 71

6. REFERENCES 72

LIST OF FIGURES

Figure 1-1. Artist's conception of pore in an activated carbon structure. 4
Figure 1-2. SEM of polystyrene foam produced using TIPS. 7
Figure 1-3. Process for making microcellular foams. T_c is the critical temperature for the liquid phase separation and T_f is the freezing point of the solvent. 8
Figure 1-4. SEM of web structure of carbon foam. 10
Figure 2-1. Proposed structure of mesophase pitch. 13
Figure 2-2. Transformation of pitch from isotropic to anisotropic phase. 15
Figure 2-3. Nematic liquid crystalline structure. 16
Figure 2-4. Three dimensional schematic of mesophase pitch. 16
Figure 3-1. Diagram of system. 19
Figure 3-2. Extrapolation of mass of CO_2 from 0 sec back to 80 sec. 24
Figure 3-3. Desorption graph of experimental data taken at temperatures between 20° C and 50° C and comparison with theoretical diffusion coefficient. 25
Figure 3-4. Comparison of heterogeneous and homogeneous nucleation rates in reference to the melting temperature of the material. 26
Figure 3-5. Graph of free energy curves against the critical radius. 27
Figure 3-6. Schematic of bubble on substrate. 28
Figure 3-7. Isothermal transformation curves where the temperature can be interchanged with pressure. 30
Figure 4-1. Normalized mass of samples dipped 15x and carbonized at 900° C. 40
Figure 4-2. Normalized mass of samples dipped 15x and carbonized at 1200° C. 41
Figure 4-3. Normalized mass of samples dipped 30x and carbonized at 900° C. 42
Figure 4-3. Normalized mass of samples dipped 45x and carbonized at 900° C. 43
Figure 4-4. % Change of 15x dipped samples carbonized at 900° C. 44
Figure 4-5. Mass % Change of 15x dipped samples carbonized at 1200° C. 45
Figure 4-6. Mass % Change of 30x dipped samples carbonized at 900° C. 46
Figure 4-7. Mass % Change of 45x dipped samples carbonized at 900° C. 47
Figure 4-8. X-ray diffraction pattern of pure graphite standard. 50
Figure 4-9. X-ray diffraction of Lexan substrate. 51
Figure 4-10. X- ray diffraction of carbonized 15x dipped foam (900° C). 52
Figure 4-11. X- ray diffraction of carbonized 15x dipped foam (1200° C). 53
Figure 4-12. X- ray diffraction of carbonized 30x dipped foam (900° C). 54

Figure 4-13. X- ray diffraction of Graphitized 45x dipped foam (carbonized 900° C).....55
Figure 4-14. X- ray diffraction of 15x dipped foam graphitized (Carbonized at 900° C).....56
Figure 4-15. X- ray diffraction of 15x dipped foam graphitized (carbonized at 1200° C).....57
Figure 4-16. X-ray diffraction of 30x dipped foam graphitized (carbonized at 900° C).....58
Figure 4-17. X-ray diffraction of 45x dipped foam graphitized (carbonized at 900° C).....59
Figure 4-18. X-ray diffraction pattern of RVC foam. 60
Figure 4-19. Graph of intensities of each graphitized sample. 61
Figure 4-20. SEM of strut cross section of dipped foam magnified 230x.....62
Figure 4-21. SEM of surface texture of dipped foam magnified 150x.....62
Figure 4-22. SEM of surface texture of oxidized foam magnified 150x.....63
Figure 4-23. SEM of strut cross section of oxidized foam magnified 200x.....63
Figure 4-24. SEM of surface texture of foam after polyurethane has been burnt out magnified 150x. 64
Figure 4-25. SEM of strut cross section of foam after polyurethane has been burnt out magnified 100x. 64
Figure 4-26. SEM of a hollow junction of carbonized foam magnified 140x.....65
Figure 4-27. SEM of a hollow junction of carbonized foam magnified 200x.....65
Figure 4-28. SEM of a solid strut of carbonized foam magnified 200x. 65
Figure 4-29. SEM of a solid strut of carbonized foam magnified 150x. 65
Figure 4-30. SEM of graphitized 15x dipped foam (carbonized at 1200° C) magnified at 650x. 66
Figure 4-31. SEM of graphitized 15x dipped foam (carbonized at 1200° C) magnified at 170x. 66
Figure 4-32. SEM of graphitized 15x dipped foam (carbonized at 900° C) magnified at 450x. 66
Figure 4-33. SEM of graphitized 30x dipped foam (carbonized at 900° C) magnified at 250x. 66
Figure 4-34. SEM of graphitized 45x dipped foam (carbonized at 900° C) magnified at 170x. 67
Figure 4-35. SEM of graphitized 45x dipped foam (carbonized at 900° C) magnified at 170x. 67
Figure 4-36. SEM of reticulated vitreous carbon foam. 68
Figure 4-37. SEM of sample C 15x. 69

LIST OF TABLES

Table 2-1. Properties of AR Resin 14
Table 3-1. Summary of diffusion coefficient for different foam systems. 22
Table 3-2. Summary of nitrogen experiments. 31
Table 3-3. Summary of CO_2 experiments using compressed pitch. 32
Table 3-4. Summary of CO_2 experiments using pitch pellets 32
Table 3-5. Summary of reblowing experiments. 34
Table 4-1. Mass summary of each run. 39
Table 4-2. X-ray diffraction peaks and corresponding interplanar spacing and intensities for pure graphite. 48

1. ORGANIZATION AND BACKGROUND

The extrème mechanical properties of carbon fibers arise from the alignment of the carbon bonds in the axial direction. They also have high temperature stability and high thermal conductivity. These properties could be advantageous in a cellular structure, where each strut would simulate a carbon fiber. The interconnected network of struts may give new applications for the foam where carbon fibers may not be of any use. Applications of carbon foams could be in the biological community for bone structures or implants, they could be used as filters, for composite reinforcement or as substrates.

The goal of this research is to produce a reticulated graphitic carbon foam with a porosity on the order of 10 pores per inch using mesophase pitch. The pitch, which was synthesized by Mitsubishi Gas Chemical Company Inc., was used because of its ability to produce high strength carbon fibers. Previously produced carbon foams are microcellular, (porosity of < 10 μm) or made of vitreous carbon, which cannot be graphitized.

The production of polymer foams has given some insight into creating carbon foams, which can be manufactured using similar techniques. The use of blowing agents are most common in the production of plastic foams. This method was modified to create a carbon foam from mesophase pitch. Two of these experiments are discussed in Chapter 3. A second method, developed for this thesis, was the dipping of an existing polymer foam in a solution of mesophase pitch (MP) and a solvent; this is discussed in Chapter 4. The first Chapter reviews manufacturing techniques of polymeric and carbon foams, and their applications. The second chapter is a discussion of high strength carbon fibers and their precursors.

1.1 INTRODUCTION

Cellular materials, commonly referred to as foams, are efficient structures for many applications and are abundant in nature i.e. wood and bone. The cellular framework gives support to the structure without adding a lot of weight and is an efficient high strength low density material.

A foam is a three dimensional two phase structure, containing a network of interconnecting struts. The network of struts creates voids in the material called cells, which maybe open or closed. The solid phase of the foam is comprised of the struts and the gas phase fills the voids between each strut. Open celled or reticulated foams allow fluid to flow in between the struts through the voids, whereas closed celled foams are generally impermeable. Foams can be made of materials such as glass, ceramics, metals, or polymers. The nature of the material is the dominant factor in determining the physical properties of the foam and will determine its flexibility or rigidity: i.e. it can be flexible, rigid, or semi-rigid.

1.1.1 APPLICATIONS OF CARBON FOAMS

Carbon foams have applications where light weight and high temperature resistant materials are required. A 3D morphology can be obtained, forming an intricate network of interconnecting struts. These struts have the potential to simulate graphitic carbon fibers with a high specific strength, high specific stiffness, high thermal conductivity, and extreme high temperature stability. Carbon foams could be used as a fugitive phase for inverse metal foams, as rapid thermal capacitors, catalyst substrates, 3D composite reinforcement, or can be activated and used for caustic and biological filters. A brief description of these potential applications is given below.

Inverse Metal Foam: The carbon is able to withstand extreme temperatures and thus can be used in the creation of metal foams. As a fugitive phase, carbon foams provide

a substrate on which to cast molten metal. After the molten metal has been cast and cooled, the carbon can then be extracted by burning it out of the metal in air at temperatures above 400° C.

Rapid Thermal Capacitor (RTC) [1]: The RTC may be useful for thermal recovery and reuse, cyclic thermal protection, temperature moderation of fuels and other liquids. A graphitic foam is impregnated with a phase change material. The potential exists to exploit the high thermal conductivity of graphite in a 3D morphology. The struts would serve as a conduction path for the heat to enter the phase change material.

Catalyst Substrates: A catalyst is placed on the struts of the foam, exposing a large surface area to the material requiring the catalyst.

Filters: Used for molten metals, corrosive chemicals, high or low temperature gases and liquids where maximum chemical inertness and good filtration is needed. Used in pollution control or to remove undesirable colors.

Biological Structures [2]: Various materials can be deposited on carbon foam to provide an excellent biocompatable matrix structure, which promotes bone growth.

Activated Carbon: An inactive carbon may be activated by heating it in steam or carbon dioxide at temperatures of 700 - 1000° C. Activation is simply the removal of tarry products from the carbon to open the pores (Figure 1-1). This creates a structure with a highly developed molecular porosity and large surface area. Opening microscopic pores in the struts of the foam gives the ability to filter undesirable molecules.

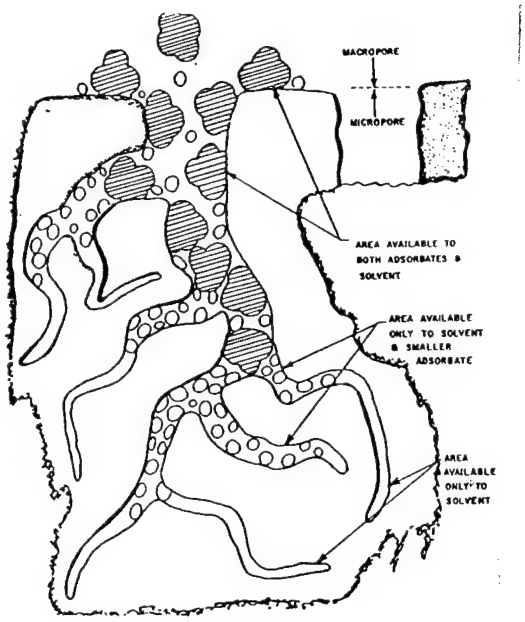

Figure 1-1. Artist's conception of pore in an activated carbon structure [3].

Composite Reinforcement: Carbon foams could be used in composite reinforcement applications by sandwiching the foam. The sandwich material could consist of graphite or other material in which the foam is able to withstand loads applied to it. Hall and Hager [4] performed semi-empirical analysis of a hypothetical reticulated carbon foam and then extrapolated the data for a variety of foams [5]. They applied a hypothetical reticulated graphitic foam to the structural efficiency from Ashby [6] and concluded that the foam would exceed the efficiency of all other foams in plate bending. The high strength, low density foam may provide a new material for structural reinforcement.

1.2 CARBON FOAMS

Carbon precursors such as polyurethane, polyacrylonitrile and mesophase pitch, have been used to create carbon cellular structures. When a carbon precursor is pyrolyzed, two different forms of carbon can be produced, vitreous and graphitic. Vitreous carbon foam is a glassy material and has been manufactured with a variety of cell structures and densities. They are used to filter molten metal, as porous

electrodes, and as high temperature insulation. Graphitic foam has previously only been produced with a microcellular morphology containing closed cells [7].

1.2.1 MANUFACTURING CARBON FOAMS

Foams of all varieties have been manufactured via mechanical, chemical or physical means [8]. Carbon foams have been created through Thermally Induced Phase Separation [9], Chemical Blowing Agents [10], a replication process [11] and polymer conversion. The foam produced with blowing agents is of importance to this research because it has the potential to form a reticulated foam. The other methods produce vitreous carbon foam or do not contain the desired morphology.

A technique of blowing polymer foams was developed at MIT [12]. This method creates a microcellular foam and involves dissolving a gas into a molded polymer at room temperature. Upon raising the temperature above the glass transition temperature of the polymer, thermodynamic instabilities are created. In doing so, the gas comes out of solution and thus nucleates bubbles. Classical nucleation theory has been applied to understand the bubble nucleation [12][13][14].

Carbon foams can be created in much the same way. The differences being that the gas is dissolved at higher temperatures and at high pressures and the material is a carbon precursor. The reduction in pressure causes bubble nucleation, while a decrease in temperature will stabilize the structure.

1.2.1.1 BLOWING AGENT

In general, polymeric foam formation involves the use of blowing agents, where a gas is dissolved in the polymer followed by the formation of gas bubbles and their subsequent growth. The polymer is saturated with a gas at high pressures. Instabilities are created when the temperature is raised above the polymer's glass

transition temperature. The instability in the system causes the gas to come out of solution. In doing so, it nucleates a myriad of bubbles, some of which may grow, given the right conditions. These conditions determine the cell morphology. The structure is stabilized when the viscosity increases, resulting in the solidification of a cellular structure.

There are two types of blowing agents. One method dispenses a gas, nitrogen (N_2) or carbon dioxide (CO_2) in a polymer. The gas is considered a physical blowing agent (PBA) because it is introduced and not produced by a reaction in the system. The second generates a gas within the polymer. The gas can be the result of a specific gas generating reaction, known as chemical blowing agents (CBA), like the formation of CO_2 when isocyanate reacts with water in the formation of water-blown flexible or rigid urethane foams [8]. Another technique is to generate a gas via thermal decomposition of chemical blowing agents, which creates N_2, CO_2 or both. Gases can also be generated by the volatilization of a low-boiling point solvent in the dispersed phase when exothermic reactions take place.

A variety of techniques are used to incorporate blowing agents in the production of foams. These techniques are employed to create a specific shape or part.

Extrusion [8]: Is used to produce foams from thermoplastic materials. Gas is dissolved under pressure and this polymer solution is extruded into a region of lower pressure where the material becomes supersaturated with the gas and phase separation occurs. The gas may be a dissolved volatile compound or other gas injected into the polymer melt stream in the extruder at elevated pressures or the gas could be produced by the decomposition of a chemical blowing agent.

Expandable Beads [8]: A volatile organic liquid such as n-pentane is dissolved or entrapped in the polymer beads during polymerization and is subsequently released upon heating. The increased temperature will cause the beads to melt together as the gas escapes producing a low density foam.

Injection Molding [8]: Polymer pellets contain a dispersed blowing agent which, when heated, decompose into an inert gas to form a cellular structure. After the pellets are saturated with the blowing agent, they are put into conventional injection machines.

1.2.1.2 THERMALLY INDUCED PHASE SEPARATION

Low density microcellular foams can be produced using thermally induced phase separation (TIPS) from polystyrene [15]. The foams produced contain a sheet-like open cell structure (Figure 1-2). Foams produced using the TIPS method have unique applications, such as multishell fusion targets for laser integration experiments [16][17].

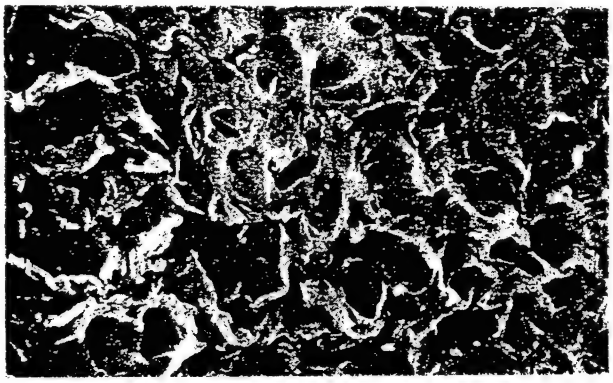

Figure 1-2. SEM of polystyrene foam produced using TIPS [18].

In general, the process of thermally induced phase separation involves the creation of a homogeneous solution by melt-blending a polymer with a high boiling, low molecular weight liquid or solid. The solution is cast into the desired shape and cooled to induce the phase separation and solidification of the polymer. The dilutent is then removed by solvent extraction and then the extractant is evaporated to yield a microporous structure.

Carbon foams can be produced by thermal decomposition of PAN, where the PAN foams have been created using the TIPS process. There are three steps in

producing microcellular foams from PAN [18]. The first step is to heat the polymer and solvent above their critical temperatures creating a homogeneous solution. The second step is to quench the solution in a controlled environment to initiate phase separation. By controlling the rate of quenching the morphology can be controlled to produce the desired structure. The third and final step is to freeze the solution which terminates the phase separation, and locks the structure in place (Figure 1-3) [19] .

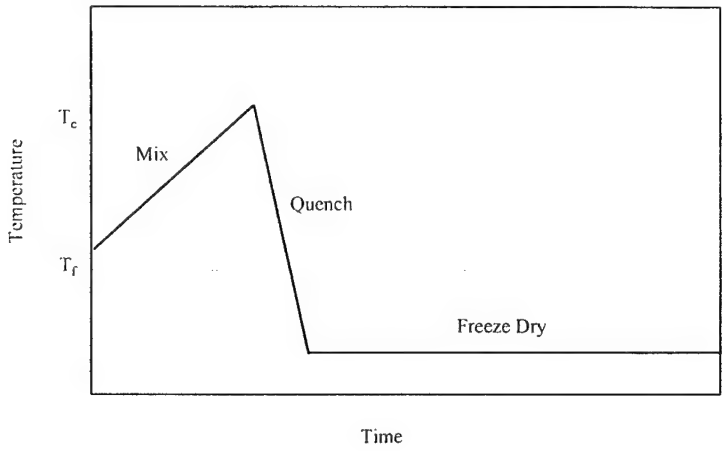

Figure 1-3. Process for making microcellular foams. T_c is the critical temperature for the liquid phase separation and T_f is the freezing point of the solvent [15].

1.2.1.3 POLYMER CONVERSION

This method involves the pyrolysis of a polymer foam, either open or closed cell. The polymer is directly converted to a reticulated vitreous carbon (RVC) foam with solid struts. Vitreous carbon contains a two dimensional structure, which can not be graphitized. Companies such as Ultramet [2] and ERG [20] have produced vitreous carbon foams with a variety of morphologies.

1.2.1.4 MESOPHASE PITCH COATED POLYURETHANE FOAM

A pre-existing foam is used as a fugitive phase to create carbon foam. Polyurethane foam with the desired morphology is dipped in a solution of mesophase pitch and a solvent. The foam is then put through a series of heat treatments to create a carbon foam with graphitic properties. The first stabilizes the pitch, the second burns out the polyurethane and the last two carbonize and graphitize the foam structure. This technique is discussed in detail in Chapter 4.

1.2.1.5 SUBSTRATE REPLICATION PROCESS

The substrate replication process produces a vitreous carbon foam with cell size on the order of 20 μm. The process involves the replication of a porous sacrificial substrate, which is used to prevent shrinkage during pyrolysis, and dictates the cell size of the foam. The substrate is made of sodium chloride (table salt) and is cold pressed into bars under 2500 psi for 3 min. The bars are then sintered in an argon atmosphere and heated to 710° C at a rate of 1° C/min. The bars are held at the set-point for 12 hours. This gives a structure with a uniform porosity. The pores are then infused with a thermosetting phenolic polymer. The phenolic solution is used as an impregnating resin because of its good solubility, low intrinsic viscosity and high carbon yield. The substrates are partially immersed in the phenolic solution, where capillary action forces the solution into the pores and prevents air bubbles from getting in the pores. The bars are then completely submerged and allowed to sit for several hours. Finally the substrates are removed from the solution and placed in an argon atmosphere furnace and heated to 700° C at a rate of 1° C/min and held for 2 h. They are then slowly cooled to room temperature, allowing the solvent to evaporate, pyrolysizing the resin within the salt substrate. The salt is extracted and then the foam is freeze dried, which leads to the final carbon foam structure (Figure 1-4).

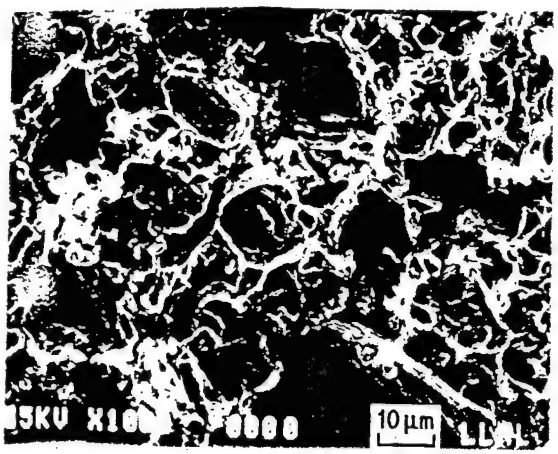

Figure 1-4. SEM of web structure of carbon foam [11].

2. CARBON FIBERS AND PRECURSORS

Producing graphitic foam requires some background of carbon fiber fabrication. The precursors used in the creation of high strength carbon fibers may also be used to create graphitic foam. The graphite structure is created by pyrolysizing the precursor several times. These heat treatment steps can be employed to the carbon foam.

Carbon fibers have extreme mechanical properties that can be attributed to the preferred orientation of the graphite crystallites with the fiber axis. The crystallite orientation is achieved by aligning the precursor molecules, followed by various heat treatments to turn the precursor into graphite. The precursors used will determine the physical properties of the final product. Therefore, in the production of carbon foams two carbon fiber precursors standout, polyacrylonitrile (PAN) and mesophase pitch (MP), which are both used to create high strength carbon fibers.

2.1 CARBON FIBER MANUFACTURING

Mesophase pitch carbon fibers are produced by extruding a molten pitch through a die. The material is wound on a winding wheel, which is at a higher velocity than the extrusion velocity and then solidified. This places a considerable amount of tension on the fiber, which aids in the alignment of the molecules in the axial direction. A three stage heat treatment process - oxygen stabilization, carbonization and graphitization - is used to further align the molecules to create high strength carbon fibers.

The microtexture of the fiber is set into place in the first stage, oxygen stabilization [21]. This is accomplished by heating the fiber in air to a temperature below the precursor glass transition temperature, usually around 240° C depending on the precursor. The stabilized fiber is then heated to a much higher temperature

(1000°C) under vacuum in the carbonization stage. These first two heat treatments remove impurities such as oxygen and hydrogen and begin to arrange the random aromatic layers into ordered graphite domains. The dominant phenomenon in the final process, graphitization, is left to structurally transform the fibers to graphite. The degree of graphitization depends on the heat treatment temperature, which is carried out at temperatures of 2000° C to 3000° C in an inert atmosphere. Graphitization is a process by which randomly stacked defective sheets are converted into perfectly stacked graphite.

2.2 PRECURSORS

There are numerous carbon precursors on the market. Organic polymers can be converted to carbon. However, when heat treated, most produce vitreous carbon, which appears amorphous and inert. The vitreous carbon has no long range crystalline structure, and can not be graphitized.

2.2.1 POLYACRYLONITRILE

Polyacrylonitrile (PAN) has been used in the fabrication of carbon fibers. It is a commercial atactic material, which has two dimensional order in the plane perpendicular to the fiber axis. There is no order along fiber axis, therefore, no true crystallization can take place [22]. When PAN is pyrolyzed in air it becomes flame-proof and highly adsorbant. It can act as a catalyst, and has some semiconducting properties.

2.2.2 PITCH

Pitch is a by-product of petroleum refining. It may come from the destructive distillation of coal or natural asphalt, by the pyrolysis of polyvinyl chloride or of a number of pure components such as naphthalene, the methylnaphthalenes, anthracene etc. Webster's dictionary defines pitch as 'a black or dark viscous substance obtained as a residue in distilling tar, wood, petroleum, etc.' [23]. A better description of pitch is a complex mixture of hundreds or thousands of predominately aromatic organic compounds with an average molecular weight of several hundred (Figure 2-1) [26].

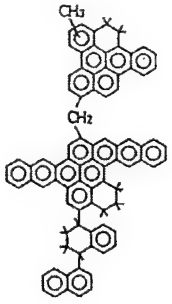

Figure 2-1. Proposed structure of mesophase pitch [24].

Pitches can be isotropic or anisotropic. Isotropic pitches are mixtures of polyaromatic molecules. They are easy to melt spin into carbon fibers, however, their modulus and strength are low [25]. Carbon fibers produced from anisotropic pitch, or mesophase pitch, have a variety of properties such as ordered microstructures, high modulus of elasticity, low electrical resistivities, and a high thermal conductivity [26]. When pitches are heated to temperatures around 400° C, they undergo dehydrogenation condensation reactions forming planar aromatic molecules which assemble into a liquid crystalline phase known as the mesophase. The ordered microstructure of mesophase pitch is closer to graphite than that found in PAN [25]. The molecular structure of mesophase pitch and its characterization is important in understanding the nature of its properties.

Much research has been done on a variety of mesophase pitches, some specifically on the pitch of interest to this research, AR Resin. Mitsubishi Gas Chemical Company Inc. produces the pitch from naphthalene without any high temperature heat treatment. The final pitch is 100% anisotropic and has the lowest softening point and highest fluidity of all mesophase pitches. It also has a higher coking value and oxidative reactivity in comparison with other pitches. Table 2-1 lists some of the properties of AR Resin. Wright Laboratory Materials Directorate at Wright - Patterson Air Force Base calculated the surface tension, γ, to be independent of temperature [27]. Mochida et al. acquired the element analysis [28] and Mitsubishi Gas Chemical Co. supplied the remainder of the properties along with the characterization of the material, stating that AR Resin is a liquid crystalline oligomer. Yoon et. al [29] determined that the mesophase pitch exhibited Newtonian flow.

Surface Tension (J/m^2)			0.035
Softening Point (°C)			238
Anisotropic Content (%)			100
Heptane Insoluble (wt %)			98.0
Toluene Insoluble (wt %)			65.1
Pyridine Insoluble (wt %)			48.0
Thermal Conductivity			400 - 600
Bulk Density (g/cm^3)			0.69
H/C (wt %)			0.6 - 0.65
Average Molecular Weight			
Pyridine Soluble (56.4%)			777
Pyridine Insoluble (43.6%)			1850
Total			1040
Element Analysis (wt %)			
Carbon	Hydroge	Nitrogen	Oxygen
94.8	4.9	0.1	0.2

Table 2-1. Properties of AR Resin.

2.2.2.1 MESOPHASE FORMATION

The formation of mesophase pitch from isotropic pitch is done by thermolysis of highly aromatic substances within temperatures of 350° C to 450° C. When the pitch changes from the isotropic phase to the anisotropic phase, the mesophase grows at the expense of the isotropic phase. This begins with the development of small anisotropic spheres in the isotropic phase (Figure 2-2). When the molecules reach a molecular weight of approximately 1000 g/mol, they are sufficiently large and flat to favor the formation of the liquid crystal or mesophase structure. As the spheres grow, they coalesce and create macroscopic formations in the bulk mesophase. Solidification occurs when the temperature is decreased. The texture of the mesophase in the advanced stages of the conversion is affected by the number of spheres and by reordering [30].

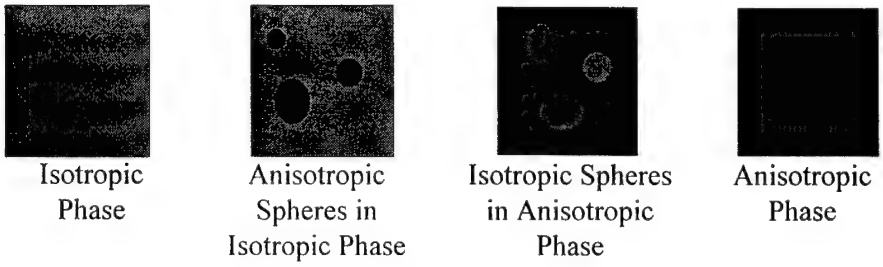

Figure 2-2. Transformation of pitch from isotropic to anisotropic phase.

MP consists of a variety of molecules consisting of soluble and insoluble fractions which provide for a fusible nematic liquid crystal structure. Liquid crystals occur when molecules align while in the liquid state and exhibit anisotropic behavior. The nematic liquid crystal (Figure 2-3) is a mobile state in which the molecules form an interlocking structure [31] and on glass surfaces, frequently adopts a characteristic threaded pattern, that is clearly visible between crossed polarizing plates. A schematic diagram of aligned MP (Figure 2-4) shows some possible molecular structures, which are irregular and contain vacant sites or holes [32].

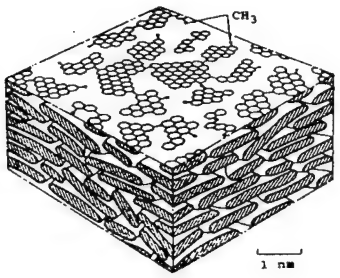

Figure 2-4. Three dimensional schematic of mesophase pitch [32].

Figure 2-3. Nematic liquid crystalline structure [31].

Mesophase pitch-based carbon fibers have superior stiffness, thermal conductivity, electrical conductivity, and have a high performance per unit weight [33]. The tensile strength of MP fibers continuously increases with heat treatment temperatures in contrast to PAN fibers [32]. Linear polymers may entangle during extension, which limits the development in the axial orientation. Whereas the stiff-like mesophase molecules make entanglement unlikely. This lack of entanglement and their short-range order, which is inherent to liquid crystals of mesophase pitch, creates extremely high degrees of axial orientation. Fibers with a high Young's Modulus are produced from MP and posses an additional degree of order corresponding to the further association of aromatic layers into well developed "sheets" with a truly graphitic structure [34].

3. PRODUCTION OF CARBON FOAMS WITH A BLOWING AGENT

The production of foams via blowing agents is a three step process: gas saturation, cell nucleation and bubble growth. Gas saturation requires dissolving a gas under pressure in a polymer creating a gas/polymer solution. A change in the pressure or temperature creates an instability in the system, which nucleates bubbles. The system will seek a lower free energy, which results in the collection of gas molecules in the form of cell nuclei. Bubble growth is dependent on the gas diffusion rate, which can be controlled by temperature and pressure [35]. Gas molecules will diffuse from the solution to nucleated cells thus making them grow, providing the viscosity is sufficiently low enough to allow material expansion. An increase in the viscosity will stabilize the foam.

Foams have been created with a variety of morphologies. To achieve a desired morphology, it is important to understand the factors affecting foam formation. The temperature of foaming, the pressure used, and the amount of time allowed to foam will all effect the final morphology of the foam.

Two different approaches were used to create a cellular structure from mesophase pitch. The first approach, direct blowing, was to use nitrogen or carbon dioxide as blowing agents. The second, reblowing, was to expand the existing structure created in the first step. The temperature of the pitch and the pressure release rate were varied in creating the foam, and were varied in both methods.

3.1 DIRECT BLOWING

The use of blowing agents in the production of reticulated carbon foam may help to align the molecules along the axial orientation of each strut. By allowing the gas to expand as bubbles are formed, the mesophase pitch molecules could be aligned

in a similar manner as carbon fibers are spun through a spinneret. Based on this idea, two different processes were tried to get the molecular alignment in the struts. The first, which is based on the same technique used at Wright-Patterson Air Force Base, is the direct blowing of the pitch.

3.1.1 PROCESS

The AR pitch is received in pellet form (average 1mm x 3mm). It was crushed in a mortar and pestle into a uniform powder and sifted through a 250μm screen. Approximately 3 g of powder was compressed under 20,000 lb to create a 35 mm x 3 mm disk. The disk was placed into a Pyrex dish sprayed with TFE release agent. The release agent allowed the foam to be removed without damage. The dish was placed in a Parr instrument company pressurized reactor vessel (model 4765) (Figure 3-1). The chamber was purged three times with the gas used. The pitch temperature was raised to a specified setpoint using an Eurotherm Corporation controller (Model 808). Once at the setpoint, the system was pressurized with the gas and allowed to saturate for a predetermined amount of time. After saturation, the controller was turned off and the pressure released. The foamed material was cooled and removed from the chamber. It was then viewed under a microscope to check for uniformity and cell density. The variations in conditions used were; temperature, pressure, gas release time, type of gas and form of pitch.

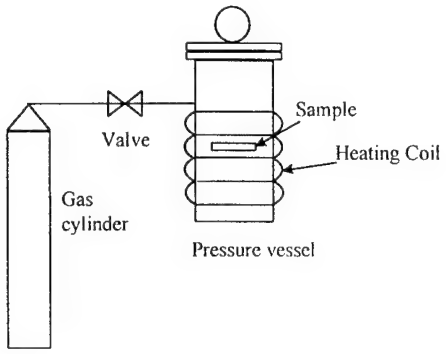

Figure 3-1. Diagram of system.

1. Crush and filter pitch
2. Compress pitch powder into disk
3. Flush chamber to create inert atm
4. Increase temperature of pitch to set-point
5. Pressurize chamber with gas
6. Saturate pitch with gas for set amount of time
7. Release pressure
8. Reduce temperature

3.1.2 GAS SATURATION

Gas saturation is the first step in producing foam. The rate of gas diffusion into the pitch will influence the gas concentration. Factors which affect the diffusion rate are the type of gas, temperature and time.

The gas is saturated in the mesophase pitch at high temperatures to increase the diffusion rate and the solubility. It is necessary to raise the temperature at which foaming will take place (foaming temperature) of the pitch to approximately 300° C. This is when the carbon plates begin to move relative to each other [36] i.e. the material is molten. The viscosity decreases allowing the gas to be saturated into the pitch, which enables the mobility of the gas molecules.

Nitrogen and carbon dioxide were used to saturate the mesophase pitch. These two gases have distinct differences which affect the diffusion rate. Nitrogen molecules are large and tend to take long periods of time to diffuse in the material.

They have to be forced in under high pressures. A plasticizer, CO_2 can be used as a softening agent, which can be absorbed in large quantities. Plasticizers can depress glass transition temperature (T_g) and reduce the viscosity of the material. Supercritical CO_2 exhibits liquid-like densities, which allows for solvent power of orders of magnitudes higher than other gases. It also has gas-like diffusivities that lead to a high rate of diffusion [37].

Experiments performed using both gases showed that the nitrogen had to be saturated at much higher temperatures than the carbon dioxide in order to produce a cellular structure. Foams produced using N_2 were created at temperatures around 310° C, where the CO_2 foam was produced at temperatures around 280° C. The CO_2 decreased the viscosity enough to foam at temperatures lower than that foamed using the nitrogen.

It is possible to calculate the gas diffusion rate into the material. This can be accomplished by periodically removing the sample from the pressure chamber and weighing it. For a period of time, the gas concentration in the material increases with increasing time. When the amount of gas reaches a maximum the material is completely saturated with the gas. The gas concentration can be experimentally determined by plotting the ratio of the mass of the gas to the mass of the pitch against time. This is referred to as the weight gain or gas uptake [38]:

$$\frac{m_g}{m_p} \tag{3-1}$$

where m_g is the mass of the gas in milligrams and m_p is the mass of the pitch in grams. The time at which it takes the gas to get to a maximum concentration in the material is the saturation time that should be used in the foaming experiments.

Another method to determine the concentration and diffusion coefficient of the gas is through a desorption experiment. This was done by saturating the material with CO_2 at temperatures between 20° C and 50° C for 8 hrs to ensure that the maximum gas concentration would be obtained. The mesophase pitch disk was quickly removed from the chamber and weighed. The mass was recorded every 20

sec for 30 min. Figure 3-2 is a plot the mass loss against time. It took approximately 80 sec from depressurization of the chamber to removal of the pitch to a precision balance. The data in (Figure 3-2) was extrapolated back 80 sec to estimate the amount of CO_2 in the system before measurements were recorded. From this data the mass concentration of the CO_2 in the pitch, x_g, was calculated using

$$x_g = \left(\frac{m_g}{m_g + m_p} \right) \tag{3-2}$$

An average was taken of the two experiments yielding approximately 3.36% CO_2.

The diffusion of CO_2 out of the pitch is modeled using a surface evaporation equation [39], where the total amount of gas diffusing out of the pitch, M_t, up to time t, is expressed as a fraction of M_∞, the corresponding quantity at time equal to zero,

$$\frac{M_t}{M_\infty} = \sum_{n=1}^{\infty} \frac{2L^2 e^{-\beta_n^2 Dt/l^2}}{\beta_n^2 \left(\beta_n^2 + L^2 + L \right)} \tag{3-3}$$

where the β_n's are the positive roots of

$$\beta \tan \beta = L \tag{3-4}$$

$$L = l\alpha / D \tag{3-5}$$

where l is half the thickness of the disk, D is the diffusion coefficient and α is a constant of proportionality, which relates to the evaporation at the surface and is assumed as unity in this case.

Values of D and β were used in (3-3) to estimate the diffusion coefficient of the CO_2/pitch system. Graphs of the mass ratio vs. time were plotted of the experimental data and the values returned using (3-3) (Figure 3-3). A diffusion coefficient of 2.0×10^{-5} cm^2/sec was the best fit value for the experimental data. A summary of diffusion coefficients for other systems is given in Table 3-1. The results show that mesophase pitch is much more permeable than high molecular weight polymers, as expected.

	Kumar, Weller, Montecillo [40]	Kumar, Weller [41]	Kumar, Weller [41]
D (cm^2/sec)	$1.3x10^{-8}$	$5.1x10^{-8}$	$4.2x10^{-8}$
Gas	CO_2	CO_2	N_2
Pressure (psi)	700	800	2000
Polymer	PVC	Polycarbonate	Polystyrene

Table 3-1. Summary of diffusion coefficient for different foam systems.

Using the value obtained for D, the saturation time needed to get the maximum concentration of CO_2 in the mesophase pitch can be determined, by again solving equation (3-3) for a gas going into the pitch. The result is 13 min to completely saturate the pitch.

The diffusion coefficient can also be used to estimate the porosity of the final foam based on a given pressure release time. Some assumptions made are;

1. Gas is lost from the mesophase pitch only during the gas release time. All the remaining gas is trapped in the foam.
2. The gas trapped in the foam expands until the bubble pressure is 1 atm.

For a given pressure release time, the mass ratio of the CO_2 is determined from Figure 3-3. The mass of the CO_2 at a given time is then determined by

$$m_g = \frac{M_t}{M_\infty} x_g m_p \tag{3-6}$$

where the mass of the pitch is known, and the concentration is assumed to be 3.36% when the pitch is completely saturated. With the mass of the CO_2, the volume can then be determined by the ideal gas law, where R = 0.08206 L atm K^{-1} mol^{-1}, T = 298° K, and P = 1 atm. The porosity is then estimated by

$$\eta = \frac{V_g}{V_g + V_p} \tag{3-7}$$

where V_g and V_p are the volumes of the gas and pitch respectively. The porosity calculated in (3-7) can be compared to the measured porosity of the foam. This is calculated by measuring the apparent density and mass of the foam. The porosity can be determined without the knowledge of mass of the gas, assuming that $m_g << m_p$;

$$\eta_a = \frac{\frac{m_T}{\rho_T} - \frac{m_p}{\rho_p}}{\frac{m_T}{\rho_T}} \tag{3-8}$$

where m_T denotes the total mass of the foam and ρ_T is the foam density. For a specimen with a pressure release time of 30 sec, the measured porosity for a foam was 79.3%. The predicited porosity using (3-7) was 69.2%. This yields 12.7% error, which is a reasonable approximation.

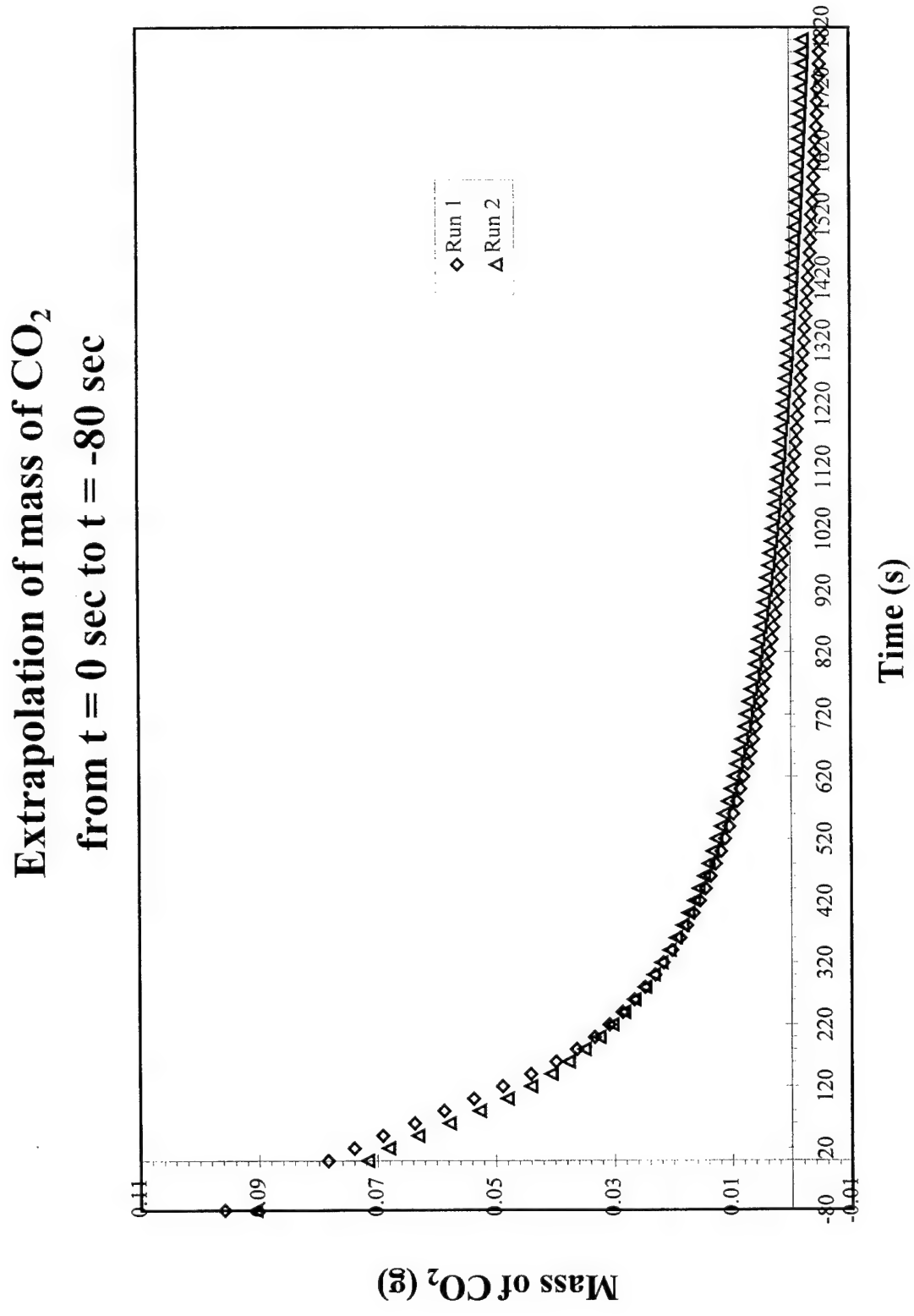

Figure 3-2. Extrapolation of mass of CO_2 from 0 sec back to 80 sec.

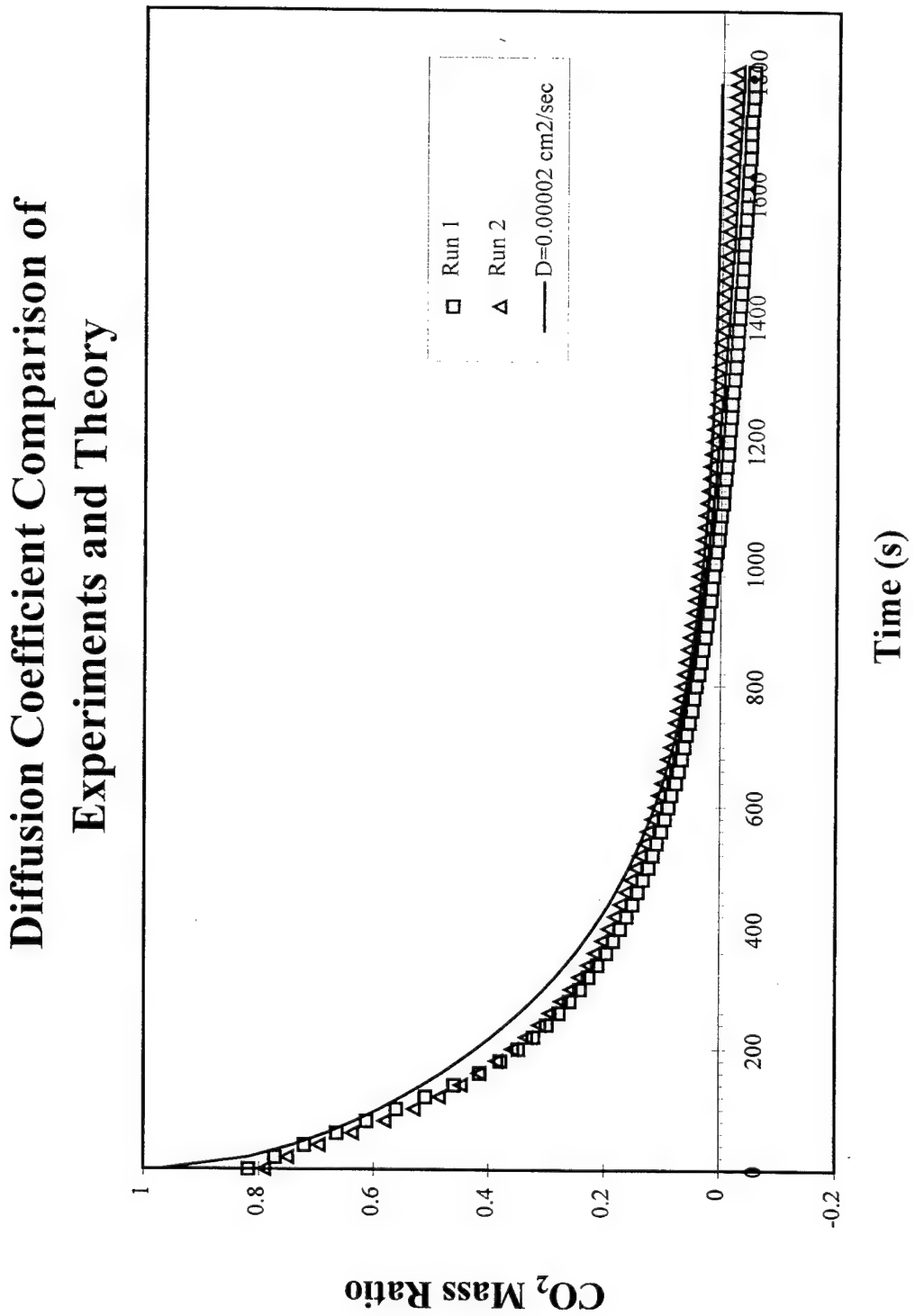

Figure 3-3. Desorption graph of experimental data taken at temperatures between 20° C and 50° C and comparison with theoretical diffusion coefficient.

3.1.3 BUBBLE NUCLEATION

Bubble nucleation can be described using classical nucleation theory, which consists of homogeneous nucleation, heterogeneous nucleation or a combination of the two. Heterogeneous nucleation is favored and will occur before homogeneous nucleation because it has a lower energy barrier (Figure 3-4).

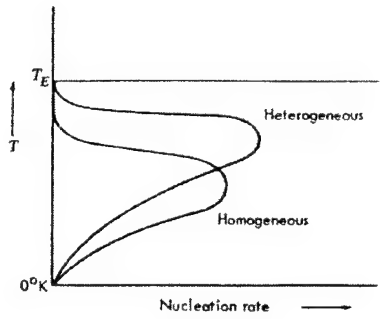

Figure 3-4. Comparison of heterogeneous and homogeneous nucleation rates in reference to the melting temperature of the material [46].

Homogeneous nucleation occurs when a sufficient amount of gas molecules come together for a long enough period of time to produce a critical bubble nucleus as in foaming of the pitch. Heterogeneous nucleation occurs when a second phase is present in the material due to an insoluble additive, nucleation agent, or on the surfaces of walls.

To nucleate a bubble the system must overcome the activation barrier. The free energy associated with making a bubble of radius r in the material is a combination of the bulk free energy and the surface energy,

$$\Delta G_t = \frac{4}{3}\pi r^3 \Delta G_v + 4\pi r^2 \gamma \tag{3-9}$$

where

$$\Delta G_v = \rho RT \ln \frac{P_s}{\Delta P} \tag{3-10}$$

and ΔP is the difference in pressure used to diffuse the gas into the material, and P_s, is the saturation pressure. The bulk free energy change involved in making the nucleus is always negative below the melting temperature of the material. The surface energy term is always positive, since energy is always expended in making an interface. Figure 3-5 shows the bulk free energy, the surface energy and the total free energy associated with the formation of a nucleus. Once a bubble nucleus reaches a critical size, r^*, it is able to grow. The critical radius is calculated by differentiating the total free energy of the system with respect to r and setting it equal to zero, resulting:

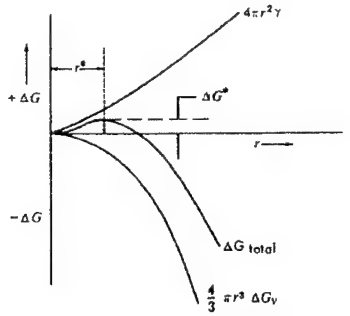

Figure 3-5. Graph of free energy curves against the critical radius [46].

$$r^* = \frac{2\gamma}{\Delta G_v} \tag{3-11}$$

where γ is the surface energy of the material-bubble interface. In order to reach this state, the bubble must attain enough free energy to get over the activation barrier , ΔG^*_{hom}, which is the Gibbs free energy associated with creating a critical size nucleus via homogeneous nucleation.

Heterogeneous nucleation can be described in a similar manner. Since it occurs on surfaces or additives in the material (Figure 3-6), it is a function of the wetting angle.

$$S(\theta) = \frac{1}{4}(2+\cos\theta)(1-\cos\theta)^2 \tag{3-12}$$

Again a critical radius is needed to create a bubble for it to grow (3-4). In this case the Gibbs free energy needed to nucleate a bubble of critical size is therefore a function of the wetting angle:

$$\Delta G^*_{het} = \frac{16\pi\gamma^3}{3\Delta P^2} S(\theta) \tag{3-13}$$

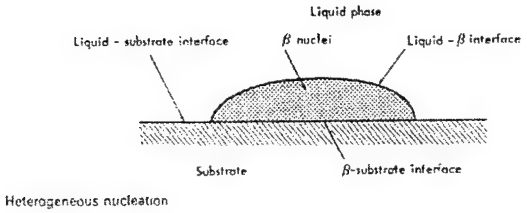

Figure 3-6. Schematic of bubble on substrate.

Since the bubble interface in this case is a liquid mixture, a correlation for the surface tension of mixtures can be employed in which the simplified form is:

$$\gamma_m = \gamma_p \left(\frac{\rho_m}{\rho_p}\right)^4 \left(1-\omega_g\right)^4 \tag{3-14}$$

where the subscripts m, p and g are the mixture, pitch and gas respectively. ρ is the mass density and ω is the weight fraction of the gas absorbed in the pitch. The large exponent (3-8) comes from the correlation for surface tension of mixtures given by Reid et. al. [42]. This can be substituted back into (3-4) to determine the critical radius needed to nucleate a bubble.

3.1.4 BUBBLE GROWTH

Once the bubbles have been nucleated then their growth must be considered. Extensive research has been conducted on the theory of bubble growth [43][44][45]. The Power Law Model is defined as a single bubble in an infinite sea of Newtonian

fluid [43]. This theory is good for bubbles spaced far apart in comparison to their radii, but not for those spaced close together. In the case of foams, this may not be a good model.

The Viscoelastic Cell Model is defined as a group of bubbles growing when closely spaced together. The creation of foams have bubbles growing closely together in relation to their radii. This theory differs from the Power Law Model in two respects: 1) If the liquid is considered infinite, the dissolved gas concentration gradient will vanish at a distance from the bubble surface. Bubbles in a foam can not exceed an equilibrium size because there is a finite supply of the dissolved gas, which is eventually depleted, thus restricting further bubble growth. 2) In a foam, bubbles are actually separated by a thin film rather than the assumed infinite fluids. The difference being that the bubble can not expand very much due to the layer of film and large mass of the liquid around it. Amon et. al. [44] describe the problems associated with this model as well as derive the required equations.

Two factors affect the diffusion of the gas to form a bubble that will grow are the driving force for the transformation, and the diffusion coefficient of the gas molecules. The driving force in the mesophase pitch system is the change in pressure, which the bubble growth is affected by the release rate of the gas pressure. The initial drop in pressure causes the gas molecules to come out of solution and form the nuclei, which subsequently grow into bubbles. As the pressure decreases the solubility of a gas decreases, so a high cell nucleation rate can be obtained when the pitch/gas solution is subjected to a rapid pressure drop. This produces many small bubbles in the pitch. In contrast, a slow pressure drop will produce fewer large bubbles. This can be seen in Figure 3-7 where the temperature can be replaced by pressure because they are roughly proportional to each other. The growth of a bubble is diffusion controlled by the rate at which the gas molecules move to form a bubble.

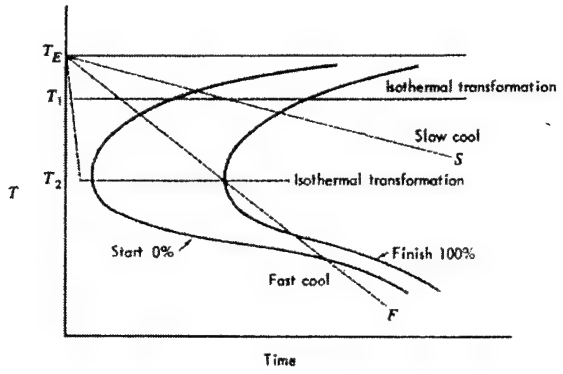

Figure 3-7. Isothermal transformation curves where the temperature can be interchanged with pressure [46].

Experiments were conducted to see how different gas release rates affected the cell size in mesophase pitch foams. As expected from the theory, when the pitch is subjected to a rapid pressure drop, many bubbles are nucleated and the cell size is small. When the pressure drop was slowed, the bubbles were larger and less numerous.

A review of nucleation phenomenon and growth gives some insight to the creation of bubbles in mesophase pitch. The temperature and pressure of the system dictate the type, number, and size of the bubbles created in the material. As the pressure is increased, the size of the critical radius needed to produce a nucleus will decrease, because the free energy is decreased (3-4). However, an increase in pressure will also decrease the size of the bubbles. This is caused by the competition of space and available gas between the bubbles. The rate at which the gas is allowed to escape from the material effects the size and number of bubbles nucleated in the foamed material. A slow pressure release will create fewer large bubbles, where a fast pressure release will cause many small bubbles to nucleate. Temperature effects cell nucleation and growth. If the temperature is low, bubbles may not form because the material is constrained and is unable to expand due to the high viscosity. However, at high temperatures, the foam may lose its structure due to collapse of the material. The viscosity in this case would be too low to maintain a cellular structure.

A balance between temperature and pressure should be acquired to achieve the desired cellular structure.

3.1.5 RESULTS

In trying to create a reticulated foam, two types of blowing agents were employed: nitrogen and carbon dioxide. Other variations included varying the temperature and pressure of the system and the gas release rate. The method of preparation of the pitch was also looked into. The first series of experiments were using nitrogen and compressed pitch. Table 3-2 lists a summary of the conditions that were altered in the nitrogen system.

Run	Temperature Set Point (C)	Gas Pressure (psi)	Saturation time (min)	Gas release time (s)	Resulting Foam Morphology
N1	300	1500	10	25	non-uniform - two cell densities
N2	310	1500	10	20	two bubble sizes factor of 2
N3	315	1500	5	20	non-uniform cell density
N4	315	1500	11	15	uniform - one bubble size (0.4 mm)
N5	310	1600	60	15	uniform - one bubble size (0.4 mm)

Table 3-2. Summary of nitrogen experiments.

Success was achieved in creating a foam with a uniform density. The conditions in run N4 were repeated numerous times and the same results were visible. A uniform cell morphology was achieved. However, the cells appeared to be closed and microcellular. In run N5, the saturation time was increased dramatically, but there was no change in the cell size.

Carbon dioxide was used as a blowing agent because of its potential plasticizing effect on the pitch. The saturation/foaming temperature was decreased about 30° C from the temperature used with nitrogen. The variations in the procedure were similar to those run with nitrogen and can be seen in Table 3-3.

Run	Temperature Set Point (C)	Gas Pressure (psi)	Saturation time (min)	Gas release time (sec)	Resulting Foam Morphology
C1	315	900	480	435	large bubbles (1 mm) non-uniform
C2	240	850	720	8	no foam
C3	260	850	720	10	uniform fine bubbles
C4	280	850	720	10	two cell densities
C5	300	850	750	10	uniform fine bubbles
C6	280	850	570	10	uniform fine bubbles
C7	280	850	60	15	uniform fine bubbles
C8	280	850	60	150	no cell structure
C9	300	850	60	210	no cell structure
C10	290	850	60	35	uniform fine bubbles

Table 3-3. Summary of CO_2 experiments using compressed pitch.

The saturation times greater than 60 min had no significant effect on the morphology, as expected from the diffusion experiments. However, the temperature was the leading factor affecting the bubble morphology. In run C8 the temperature dropped too quickly when the pressure was released. This kept the bubbles from growing due to the high viscosity. In contrast, the temperature in run C9 was too high resulting in a collapse of the structure. Bubbles may have formed, however the viscosity was too low, which inhibited the stabilization of the foam. The material was foamed, however there was no cellular structure because the viscosity was too low to lock in the morphology.

A new variation was added to the CO_2 system. This included the use of pitch pellets. They were not compressed as in the first two cases. This variation was executed on the basis that the pellets would melt together. On doing so, pockets of trapped gas would be create larger bubbles. Table 3-4 summaries the results of these experiments.

Run	Set Point (° C)	Pressure (psi)	Saturation time (min)	Gas release time (s)	Morphology
C11	280	850	60	50	uniform bubbles
C12	280	850	120	100	uniform large bubbles
C13	280	850	120	20	two cell densities

Table 3-4. Summary of CO_2 experiments using pitch pellets.

There was a difference in the use of the two different gases. This is largely seen in the processing conditions. The temperature and pressure used to foam the pitch were lower with carbon dioxide as compared to nitrogen. The pressure release rate made a significant difference in the size of the bubbles (μm vs. mm) however, the larger bubbles were less uniform. The lack of control of the pitch temperature made it difficult to stabilize the cellular morphology. There was no significant difference in the bubble size between the compressed pitch and pitch pellets.

3.2 REBLOWING

The method of reblowing entails creating pitch foam using the methods already mentioned and then placing it back into the chamber a second time. The blowing would, it was hoped, enlarge the existing bubbles and further align the molecules in the axial direction of the struts.

3.2.1 PROCESS

The reblowing technique is vary similar to the direct blowing method. Here the chamber was again purged three time with nitrogen or carbon dioxide. The pitch was brought up to set-point and pressurized with the gas. A summary of the steps involved is found below. The idea is to fill the already existing bubbles with the gas at a temperature where the pitch was soft enough to foam without collapsing the structure.

1. Place foamed sample in chamber
2. Flush chamber to create inert atmosphere
3. Increase temperature to set-point
4. Pressurize once at set-point for a length of time
5. Release pressure
6. Decrease temperature

The foam created in the direct blowing process was used for the reblowing. It was broken into large pieces and the cellular structure recorded. This was done to enable a comparison in the morphology before and after reblowing. The foam used for reblowing was created with both types of gases. Both carbon dioxide and nitrogen were used to reblow the material.

3.2.2 RESULTS

Foam samples containing a uniform morphology were recreated using the direct blowing method, which were then used in the reblowing process. Table 3-5 lists the conditions for each run.

Run	Temperature Set Point (C)	Gas Pressure (psi)	Saturation time (min)	Gas release time (sec)	Type of Gas	Resulting Foam Morphology
R1	320	1500	70	20	N_2	no change
R2	320	1500	29	20	N_2	no change
R3	315	1500	58	20	N_2	bubbles slightly larger
R4	305	1500	79	20	N_2	no change
R5	280	850	30	12	CO_2	structure collapsed
R6	245	850	60	10	CO_2	broke into pieces
R7	260	850	240	10	CO_2	broke into pieces and collapsed
R8	270	850	480	11	CO_2	broke into pieces and collapsed

Table 3-5. Summary of reblowing experiments.

There was difficulty in achieving a good foaming temperature. A variety of temperatures were used and to no avail. No real change in morphology was accomplished. The cellular structure was broken into many pieces or the original morphology was lost due to a collapse in the cellular structure. There was no effect on the cell structure with a change in foam used or gas used to reblow.

3.3 CONCLUSIONS

These two methods of blowing foam produced a foam, however, it did not contain desired cell density. The structure that was created was a closed cell foam with a fine cell morphology (0.4 mm). Slightly larger cells (1 mm) were created but with no uniformity to the structure. There is potential to produce a graphitic foam with the direct blowing method if the system conditions are more precisely regulated. Experiments may be continued with better control of the pitch temperature and pressure release of the gas.

Further work needs to be completed quantitatively with the use of blowing agents. The size and number of bubbles should be determined and checked with theoretical calculations to determine the type of nucleation and bubble growth phenomenon. Better understanding of the pitch properties is also needed. Density, viscosity and surface tension will all aid in accurate calculations of nucleation and bubble growth.

4. COATED POLYURETHANE FOAM

Foams can be created by using an existing cellular structure as a fugitive phase. A fugitive phase foam is used only for its structure and is then discarded, usually by burning it out of the material. This thesis proposes that graphitic foam might be produced in a similar manner. The use of a flexible polyurethane foam as the fugitive phase gives the ability to choose the cellular structure. It is abundant and is available in a wide range of cellular densities. The relatively low melting point of the polyurethane foam allows it to be extracted with ease.

4.1 PROCESS

The polyurethane foam is coated with a mesophase pitch solution. The polyurethane is then burnt out, leaving behind a pitch cellular structure that can be converted to graphite. The process consists of six steps, which are summarized below.

1. Create a solution of pitch and pyridine
2. Dip polyurethane foam in solution
3. Oxidize coated foam at 240° C for 8 hrs in air
4. Burn out polyurethane at 290° C for 8 hrs in air
5. Carbonize foam at 900° C or 1200° C for 20 hrs under vacuum
6. Graphitize foam at 2400° C for 30 min in inert atm

The flexible polyurethane foam was acquired from New Dimension Industries, Inc. (lot # 0880-2). A 10 ppi density foam was used to obtain a similar density in the graphite foam. It was important to find the temperature at which the polyurethane foam would breakdown for the burn-out process. This was accomplished by heating the polyurethane foam in air. At about 290° C the foam began to breakdown. It lost its structure and collapsed under its own weight. When the temperature was brought up even further (900° C) the foam vaporized in seconds.

4.1.1 COATING

The first stage is to coat the polyurethane foam with a solution of pitch and solvent. Pyridine, as a solvent, was chosen based on the information obtained from Mitsubishi Gas Chemical Co. (Table 2-1). It was selected because the pitch was more soluble in the pyridine than toluene. A solution of 12 g mesophase pitch and 5 mL pyridine was created to dip the foam. The solution was mixed and then filtered through a coffee filter to ensure the pitch was completely dissolved. The solution was kept covered to ensure the pyridine would not evaporate during the dipping process.

Pieces of foam were cut into pieces and weighed before dipping. The samples were dipped 15, 30, and 45 times. They were allowed to dry between each dip and then dipped again. This was done to see if more pitch could be coated on the struts, and if so if it would make a difference in the final foam. The samples were then weighed and heat treated.

4.1.2 HEAT TREATMENT

Three of the four heat treatment steps used are standard in the production of carbon fibers. The first, oxidization stabilization was carried out in an Applied Test Systems, Inc. oven. Stabilization was done in air at 240° C and held for eight hours. The samples were then removed for weighing and placed back in to be heated again. It was necessary to add this additional heat treatment step before carbonizing the foam to remove as much of the polyurethane as possible from the sample. The oven temperature was set at 290° C to burn out the polyurethane foam. The foam was left in the oven for eight hours. The samples were again weighed. The next step was to carbonize the foam samples. This was done in a Centorr Associates, Inc. furnace, which is capable of achieving temperatures of 1200° C in an inert atmosphere. All samples were treated at 900° C and held at that temperature for 20 hours at 10^{-6} torr. A portion of the 15x dipped samples were treated at 1200° C to see if a higher heat

treatment would make a difference in the structure. The heating rate for each run was about 2° C/min. All samples were then graphitized in an argon atmosphere at 2400° C. The heat rate was 45° C/min and they were held at 2400° C for 30 min.

4.2 RESULTS

The final foam contained an open celled morphology. The cell size varied between 2 mm - 3 mm and the strut thickness is estimated to be about 0.4 mm. The starting polyurethane foam was a 10 ppi density. The graphitic foam approximately doubled in density, resulting in an 18 ppi - 20 ppi foam. This change in cell density is due to the shrinkage associated with the heat treatment process. With each heat treatment step the mass changes, and based on the final cell density, the volume probably changes as well. The foam volume was not measured between each step due to the brittleness of the foam.

The foam mass increases after dipping, which is due to the addition of mesophase pitch on the struts of the foam. Upon heat treatment, however, the mass decreases. It isn't until the burn out stage that the mass of the foam falls below its initial weight. This is due to the removal of the polyurethane. The mass loss in the other heat treatment stages is due to the loss of the non-carbon elements. A summary of each run is listed in Table 4-1 and the normalized masses are plotted in Figure 4-1 - Figure 4-3. The samples carbonized at 900° C and 1200° C show no substantial difference in the mass loss. The percent change is plotted for each heat treatment in Figure 4-5 - Figure 4-8. The percent change in mass is calculated as;

$$\%\Delta = 100\left(\frac{m_f - m_o}{m_o}\right) \tag{4-1}$$

Sample	Starting Mass (g)	Dipped Mass (g)	Oxidized Mass (g)	Burn Out Mass (g)	Carbonized Mass (g)	Graphitized Mass (g)
3R3[@]	0.130	0.149	0.108	0.063	0.038	0.033
4R3[@]	0.134	0.150	0.111	0.065	0.036	0.032
5R3[@]	0.112	0.117	0.090	0.056	0.033	0.029
6R3[@]	0.104	0.117	0.090	0.054	0.031	0.028
2R4[*]	0.144	0.187	0.146	0.109	0.063	0.054
3R4[*]	0.124	0.160	0.126	0.094	0.049	0.046
1R5[*]	0.182	0.220	0.145	0.074	0.038	0.034
2R5[*]	0.181	0.225	0.143	0.071	0.041	0.040
3R5[*]	0.177	0.215	0.140	0.073	0.040	0.036
5R4[#]	0.160	0.201	0.163	0.122	0.069	0.060
6R4[#]	0.126	0.157	0.128	0.094	0.054	0.050
4R5[#]	0.214	0.275	0.194	0.112	0.064	0.053
5R5[#]	0.167	0.217	0.155	0.093	0.054	0.049
6R5[#]	0.209	0.271	0.187	0.106	0.065	0.055
8R4[$]	0.133	0.192	0.146	0.112	0.064	0.058
9R4[$]	0.160	0.219	0.166	0.127	0.068	0.065
7R5[$]	0.196	0.232	0.177	0.102	0.056	0.047
8R5[$]	0.160	0.204	0.165	0.112	0.065	0.061
9R5[$]	0.190	0.218	0.163	0.089	0.049	0.043

Table 4-1. Mass summary of each run.

[@] Dipped 15 times, carbonized at 900° C.
[*] Dipped 15 times, carbonized at 1200° C.
[#] Dipped 30 times, carbonized at 900° C.
[$] Dipped 45 times, carbonized at 900° C.

Comparing each sample after dipping shows that the samples dipped 15x and carbonized at 1200° C gained approximately two times as much mass compared to the samples dipped 15x and carbonized at 900° C. The same is true for the samples dipped 30x, whereas the 45x dipped samples gained approximately 2.5 times more mass. As the different types of foams were heat treated, the mass was decreased. The mass lost for each type of sample run after oxidization and polyurethane burn out was approximately 0.3 g. Following carbonization and graphitization the mass lost in each run was about 0.35 g and 0.05 g respectively. This demonstrates that the loss of mass is related to the processing conditions of the foam.

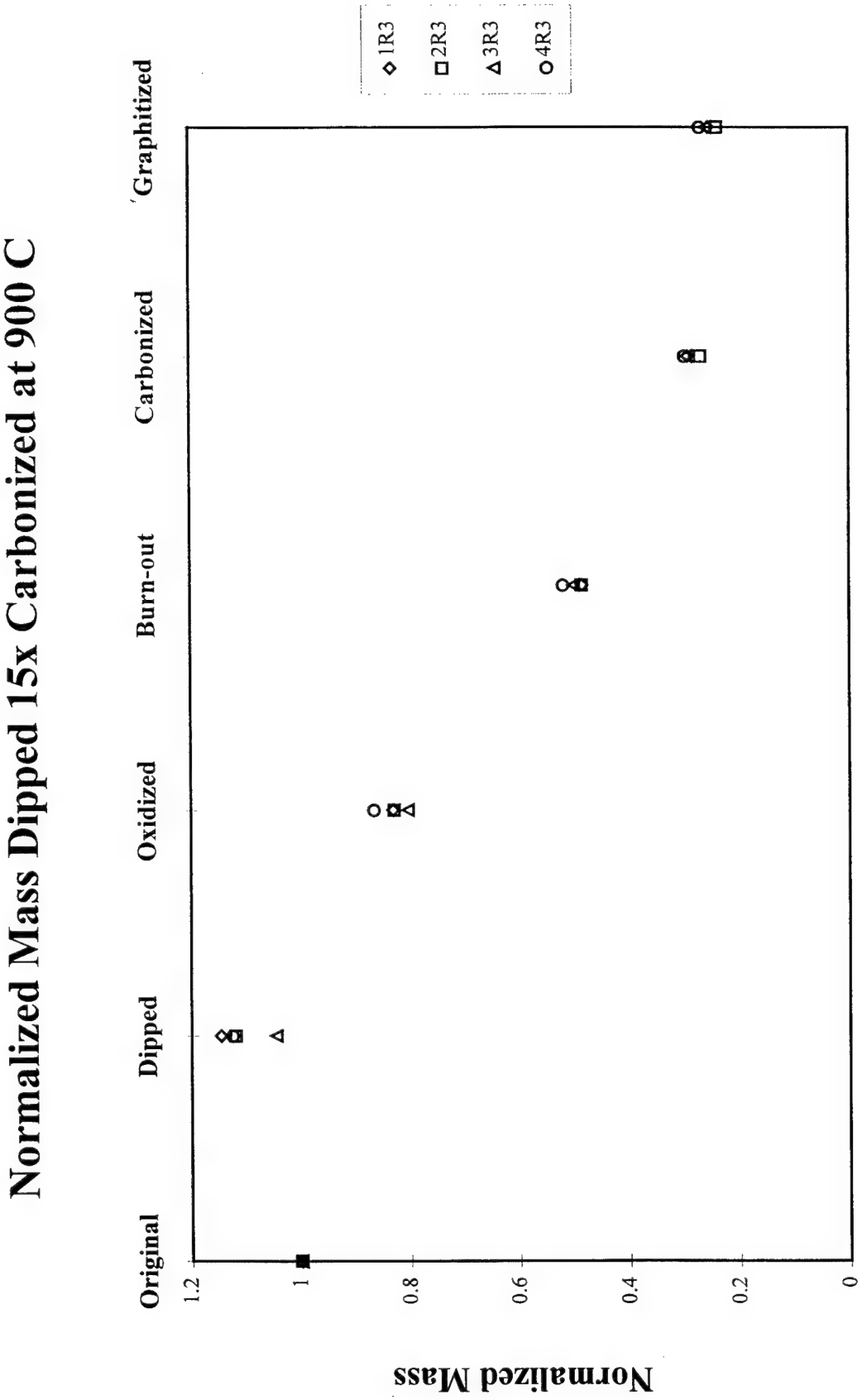

Figure 4-1. Normalized mass of samples dipped 15x and carbonized at 900° C.

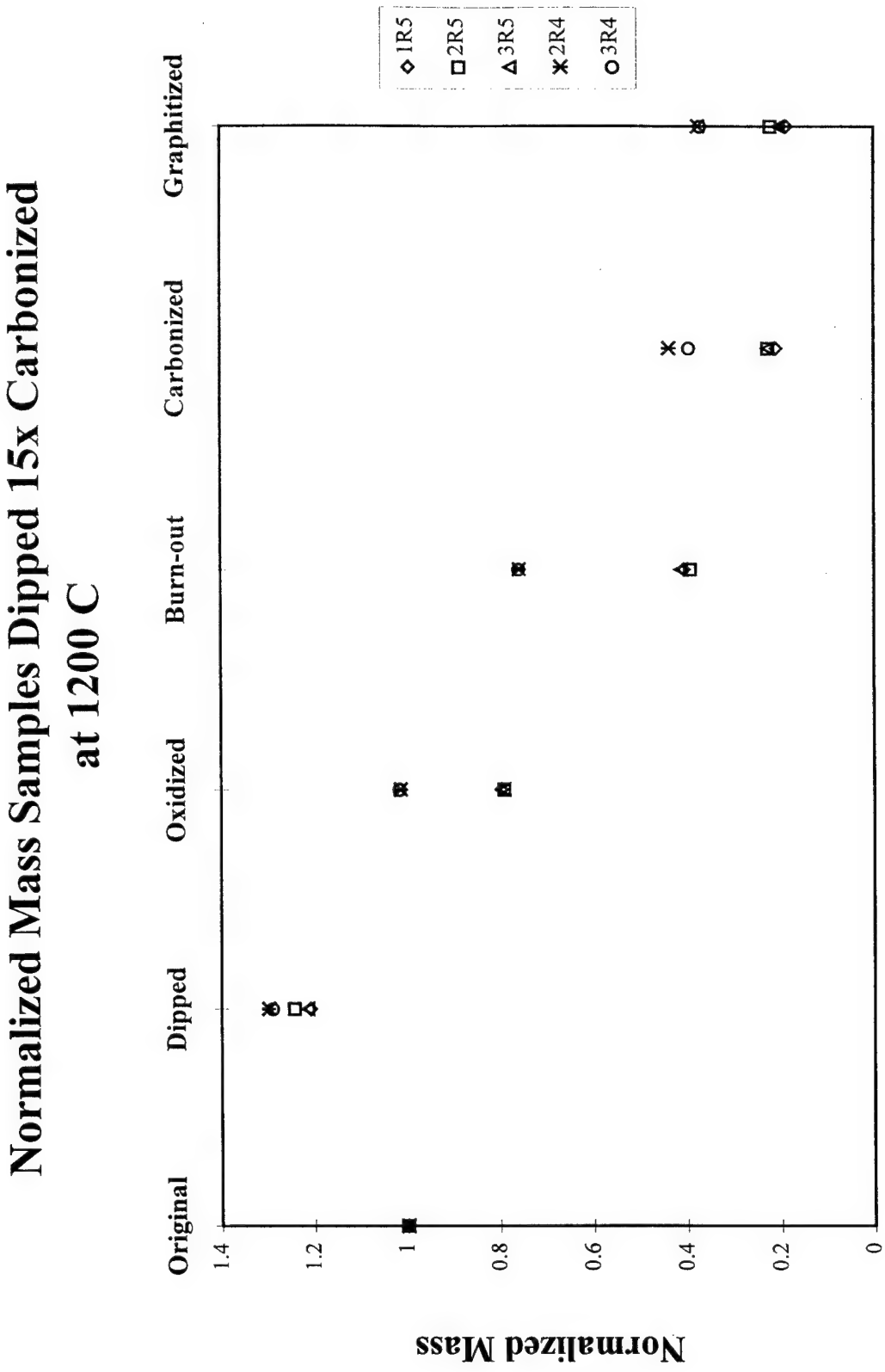

Figure 4-2. Normalized mass of samples dipped 15x and carbonized at 1200° C.

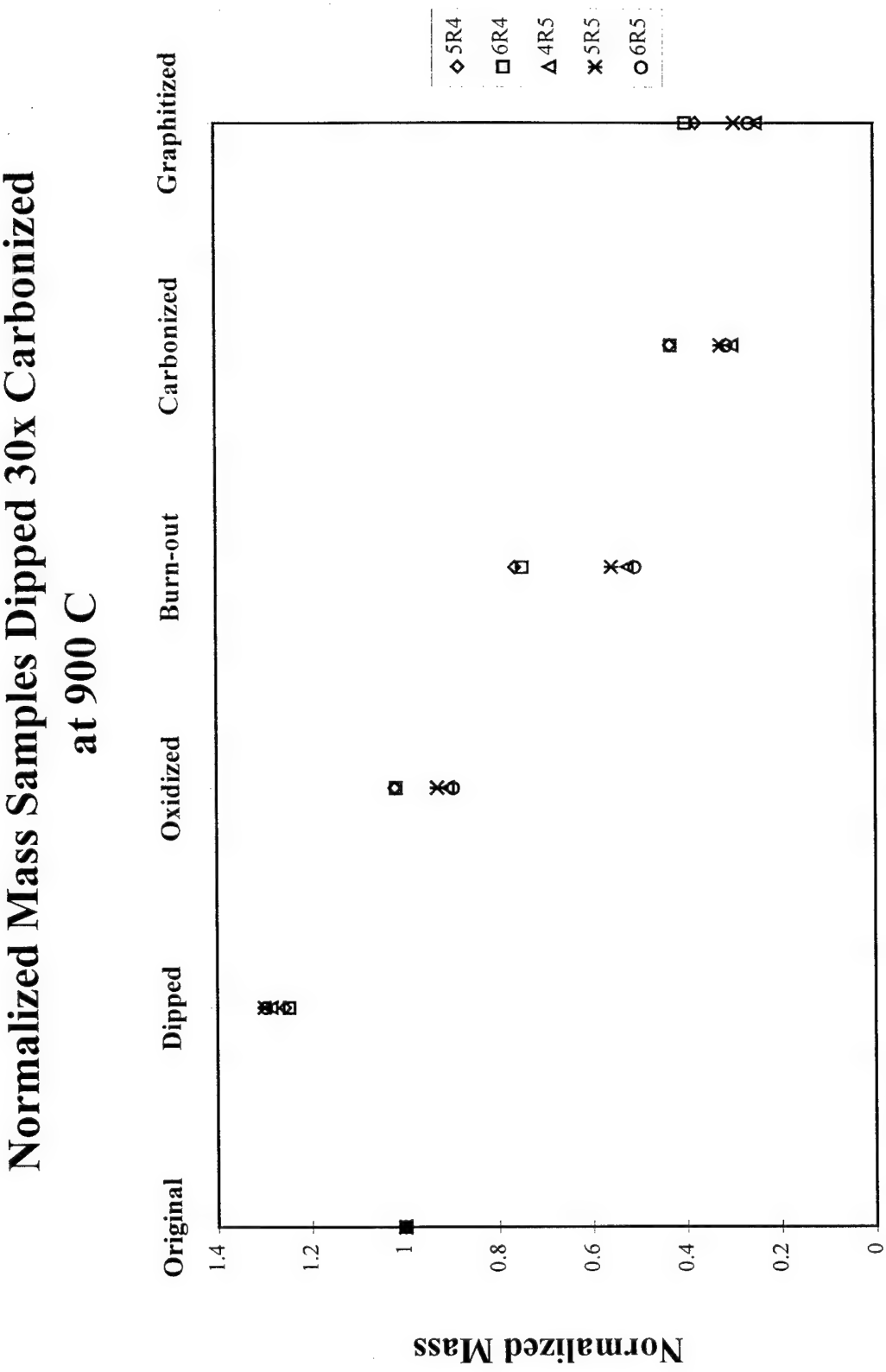

Figure 4-3. Normalized mass of samples dipped 30x and carbonized at 900° C.

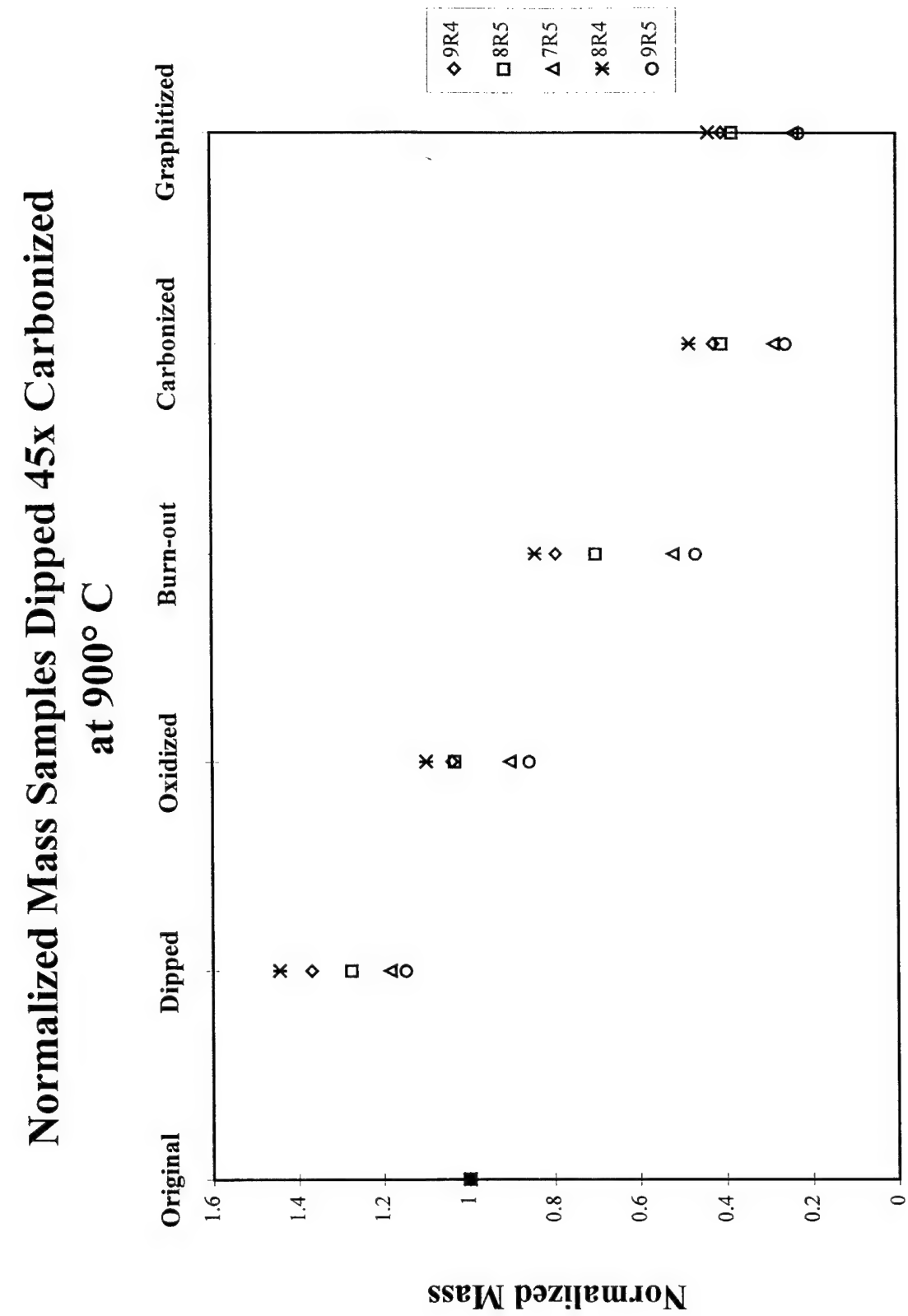

Figure 4-4. Normalized mass of samples dipped 45x and carbonized at 900° C.

Figure 4-5. % Change of 15x dipped samples carbonized at 900° C.

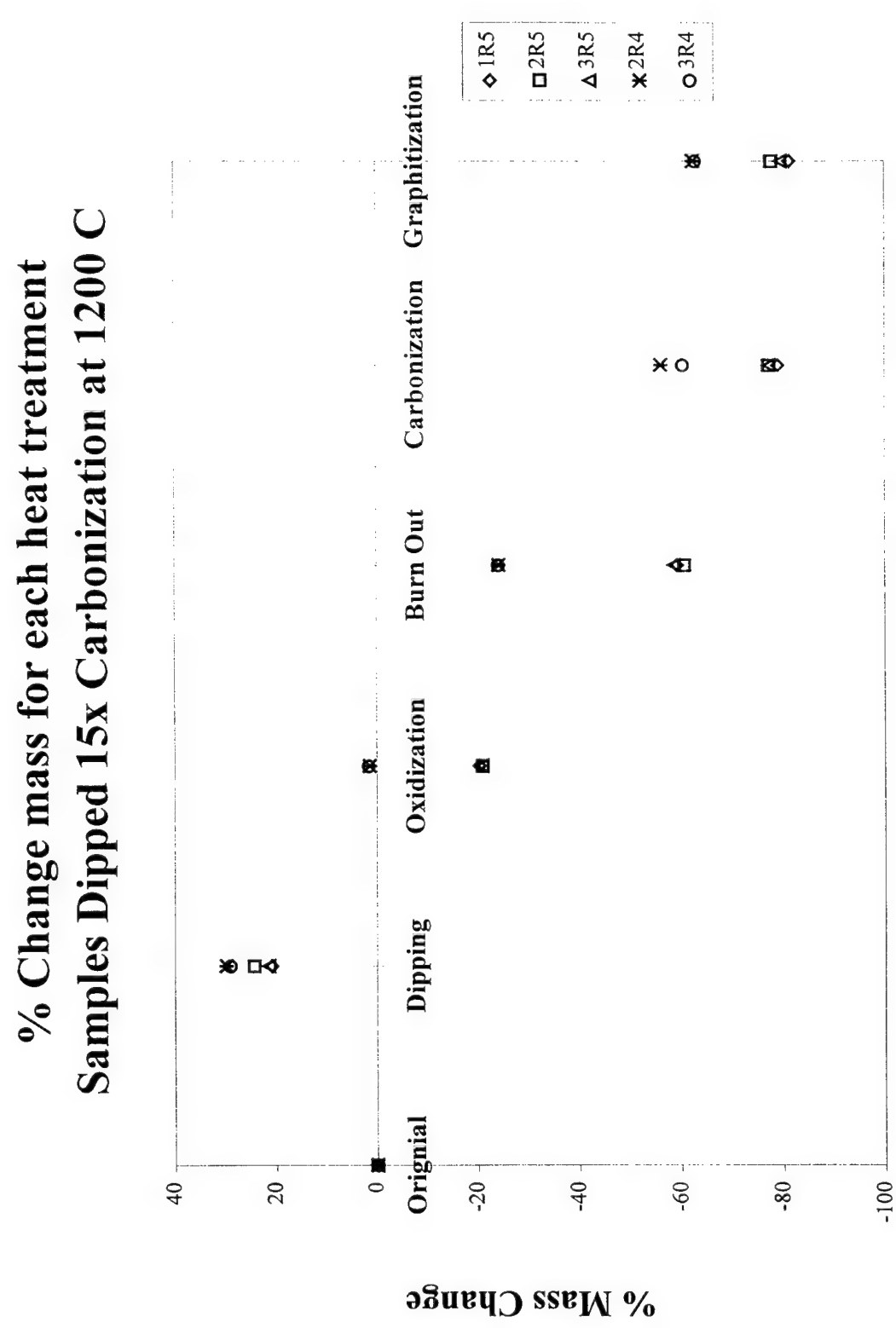

Figure 4-6. Mass % Change of 15x dipped samples carbonized at 1200° C.

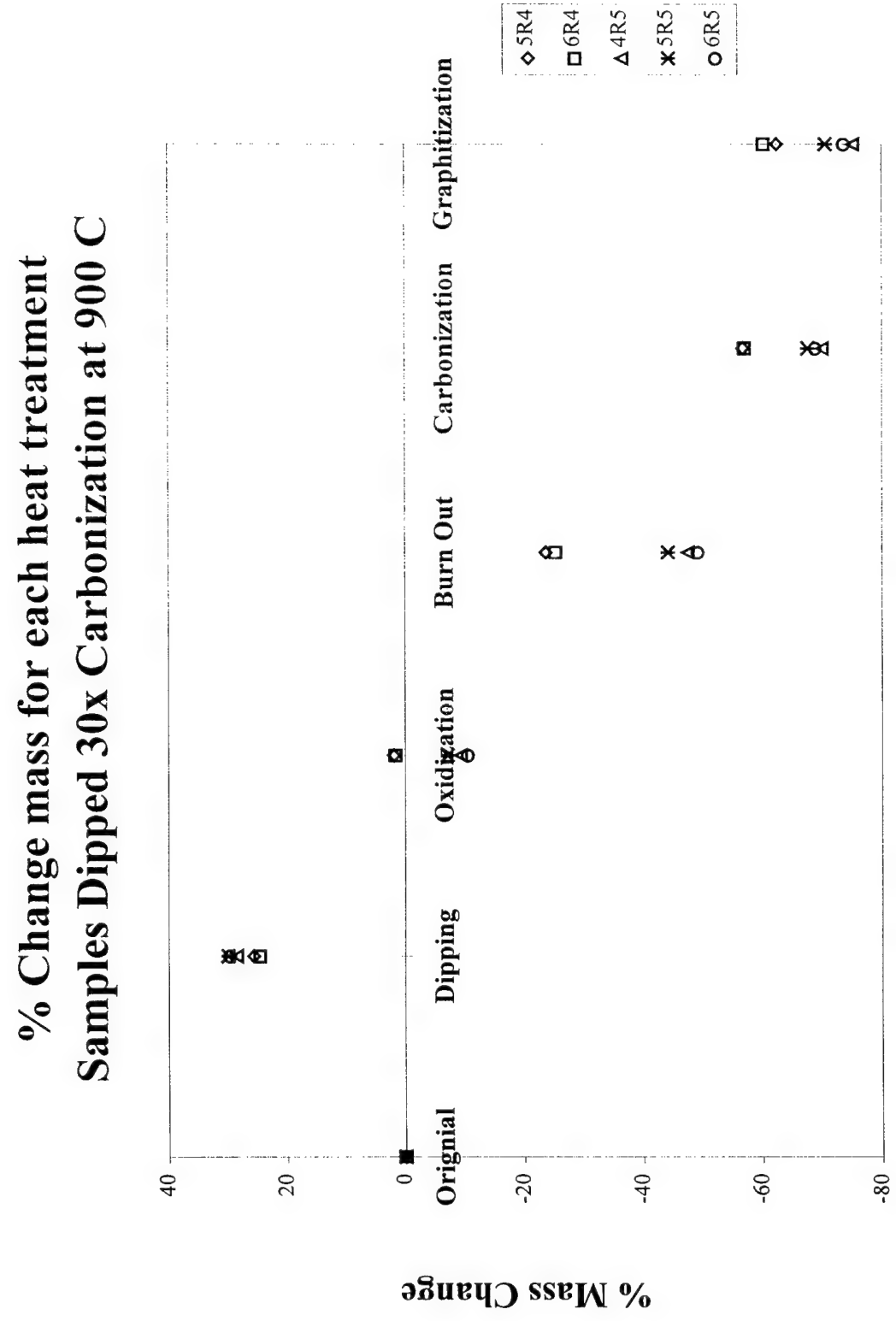

Figure 4-7. Mass % Change of 30x dipped samples carbonized at 900° C.

Figure 4-8. Mass % Change of 45x dipped samples carbonized at 900° C.

4.2.1 X-RAY DIFFRACTION

X-ray diffraction can be used to give qualitative and quantitative information on the crystalline structure of a material. In the present case, the intensity of the peaks reveal the presence of graphite crystals. X-ray analysis was completed using a D-500 Siemens Diffractometer on the carbonized and graphitized foams produced and then compared to that of a pure graphite standard, which was analyzed for indication of graphite being present in the foam samples.

The x-ray diffraction pattern of the pure graphite standard (Figure 4-9) shows the peak of highest intensity at the angle 2θ of 26.518°. This is derived from the spacing between graphite sheets and is the designated (002) peak with a interplanar spacing of 3.355 Å. A second peak (100) is related to the spacing between carbon atoms within a sheet and is observable in all annealed carbons. The peak at (101) is related to the extent to which extensive graphite sheets are in ABA order. Only carbons which show a definite (101) peak can really be defined as graphites [47]. However, in the x-ray diffraction pattern of pure graphite, it is difficult to distinguish the (100) and (101) peaks due to the high intensity of the (002) peak. Comparing the x-ray diffraction patterns of each sample only the (002) peak will be discussed, since it is easily identified.

Peak	Interplanar Spacing	Intensity
(002)	3.37 Å	100%
(110)	2.132 Å	5%
(101)	2.036 Å	2%

Table 4-2. X-ray diffraction peaks and corresponding interplanar spacing and intensities for pure graphite.

A qualitative representation of the degree of orientation of graphene planes may be obtained using x-ray diffraction. The foam samples were crushed into fine particles and placed on a Lexan substrate for x-ray analysis. The Lexan was used because it is amorphous. However, x-ray diffraction was performed on it and the result was some scatter as seen in Figure 4-10. The x-ray diffraction analysis can only be used qualitatively in that graphite is present in the foam and can be seen in the

diffraction patterns. The intensity is not very high as compared to the graphite standard, which may be attributed to a low concentration of graphitic crystals in the foam.

The diffraction patterns were plotted with the normal background removed. A comparison was done of each foam diffraction pattern with the Lexan, pure graphite standard and vitreous carbon. The cluster of peaks found on the Lexan diffraction pattern at angles 2θ of 10° to 24°, also are apparent in each sample's x-ray diffraction pattern. However, this cluster of peaks does not appear in the pure graphite diffraction pattern, which is due to the high intensity of the (002) peak. The x-ray diffraction pattern of the Lexan is plotted on the individual foam sample diffraction patterns for a comparison. The plots are scaled to include only the region of interest angles 2θ of 5° to 45°. This gives a better representation of the difference of the graphite peak vs. the Lexan peak.

The carbonized samples were x-rayed for signs of graphite formation (Figure 4-11 - Figure 4-14). The diffraction pattern of each foam is plotted with the Lexan. This was done to compare the Lexan diffraction pattern with the foam diffraction patterns. Both of the 15x dipped samples contain a peak near the angle 2θ of interest. These peaks, however are not very strong in comparison to the graphite standard. The two samples dipped 30x and 45x shows that the (002) peak is not visible. This demonstrates that the carbonized samples contain a small amount of graphite. The intensities of each carbonized and graphitized foam sample are plotted in Figure 4-20.

The graphitized foam diffraction patterns reverse roles. The samples dipped 30x and 45x show a higher (002) intensity than the samples dipped only 15x. In fact The intensity of the 15x dipped samples decreased from the carbonized samples. The x-ray diffraction patterns of each foam are plotted in Figure 4-15 - Figure 4-18.

To demonstrate the graphitized foam does contain some crystalline structure, a comparison was done with reticulated vitreous carbon foam. The x-ray diffraction of the RVC foam (Figure 4-19) is identical to that of the Lexan tray holder. RVC has no long range crystalline order and should not give an x-ray diffraction pattern.

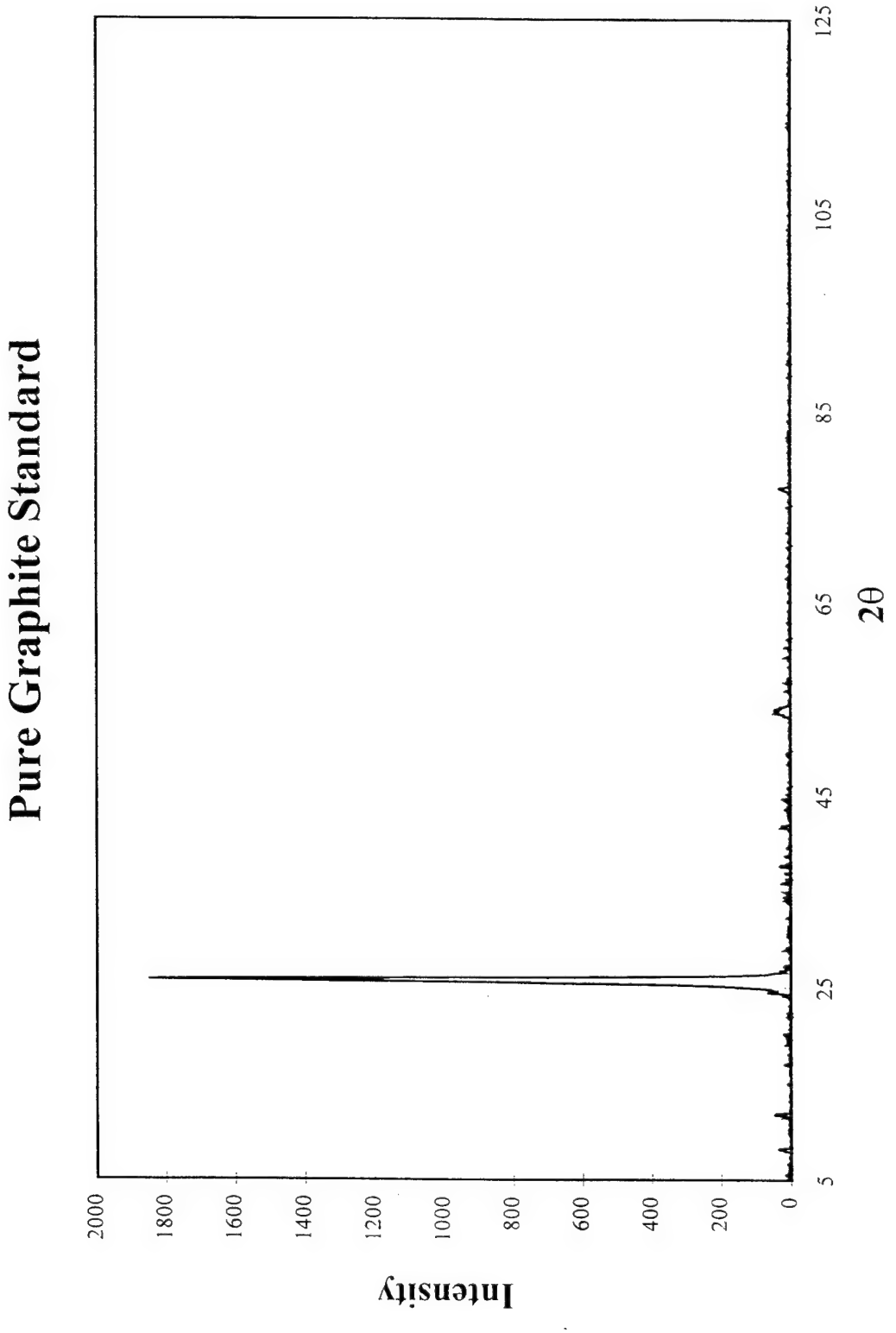

Figure 4-9. X-ray diffraction pattern of pure graphite standard.

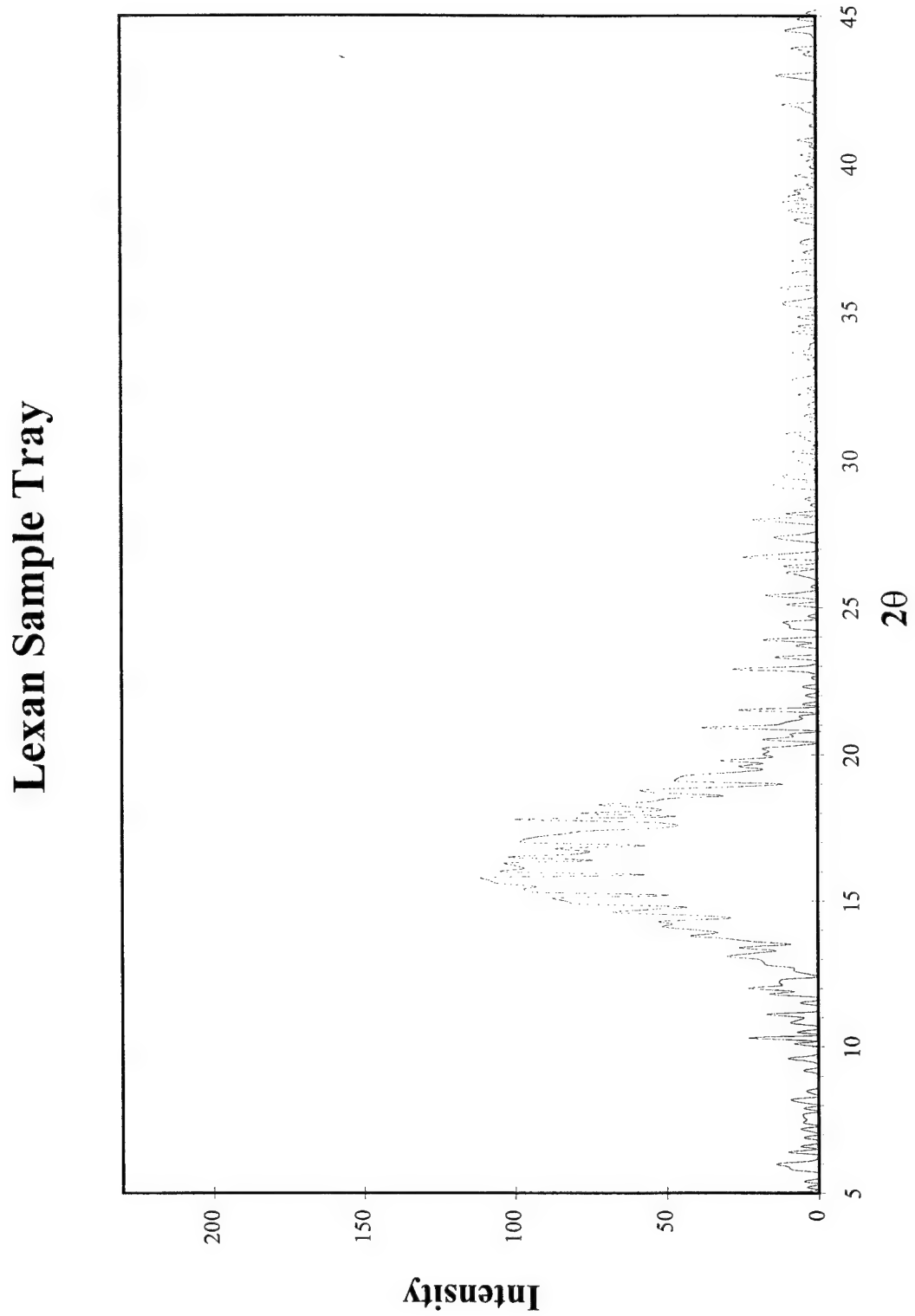

Figure 4-10. X-ray diffraction of Lexan substrate.

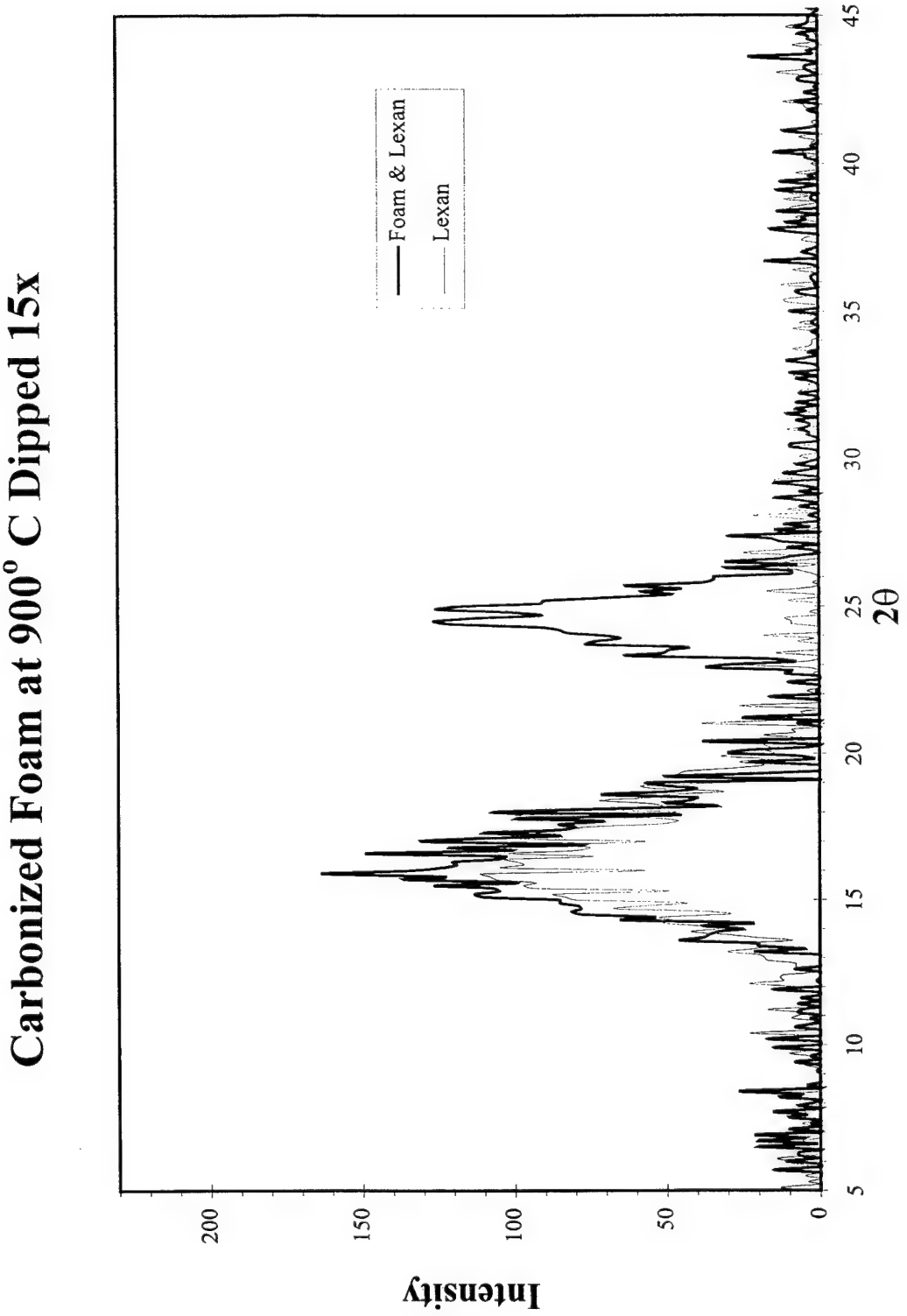

Figure 4-11. X- ray diffraction of carbonized 15x dipped foam (900° C).

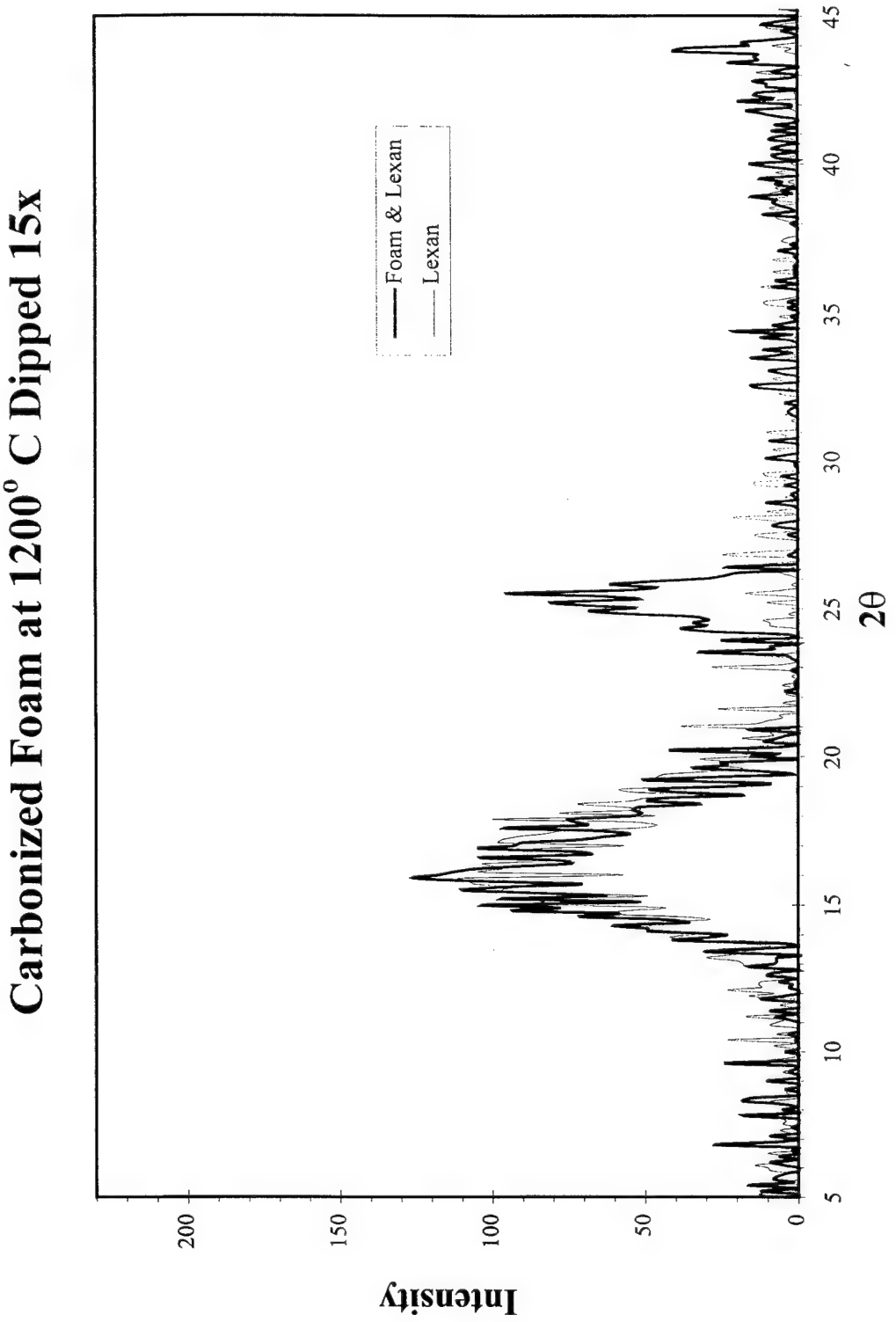

Figure 4-12. X- ray diffraction of carbonized 15x dipped foam (1200° C).

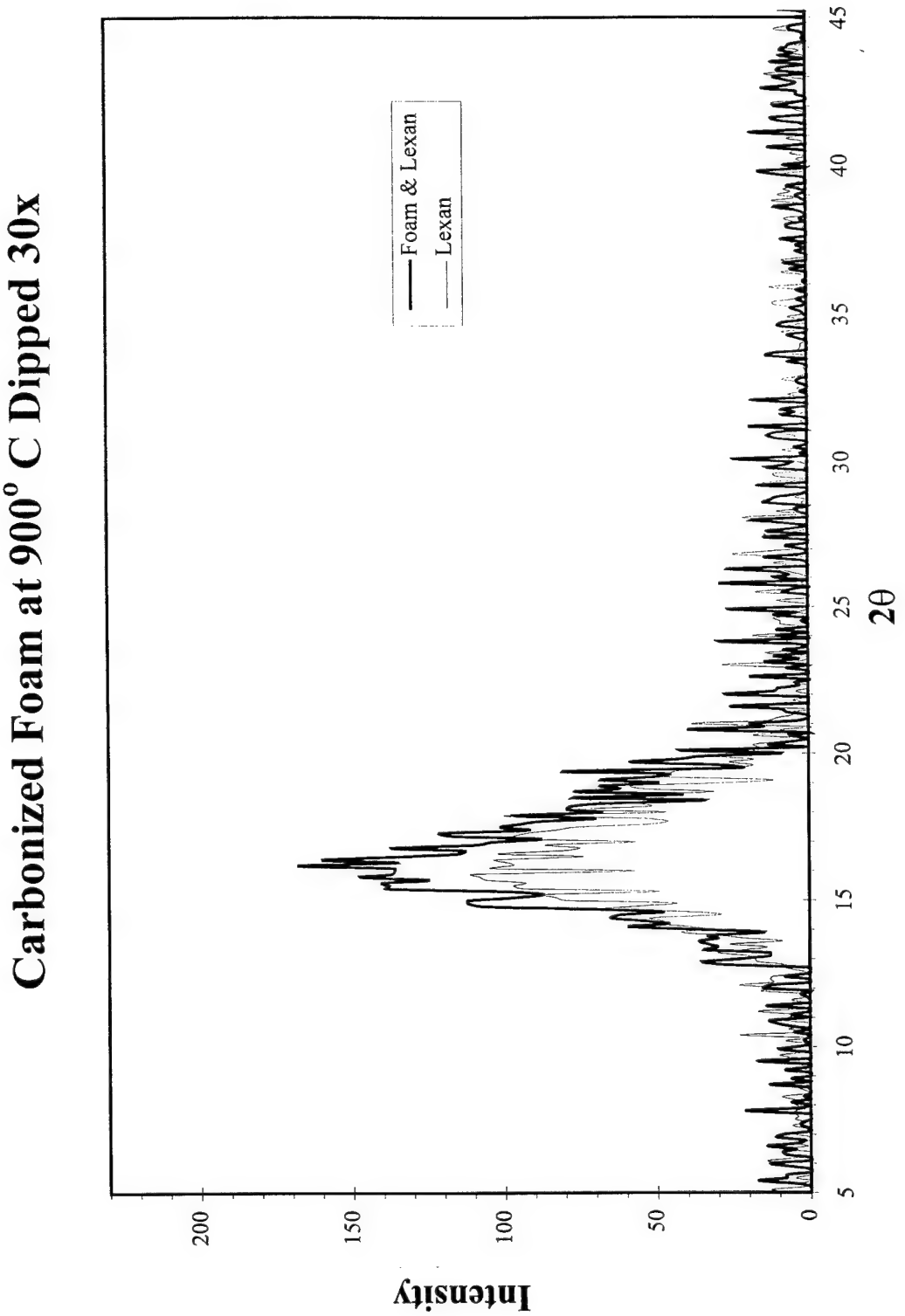

Figure 4-13. X- ray diffraction of carbonized 30x dipped foam (900° C).

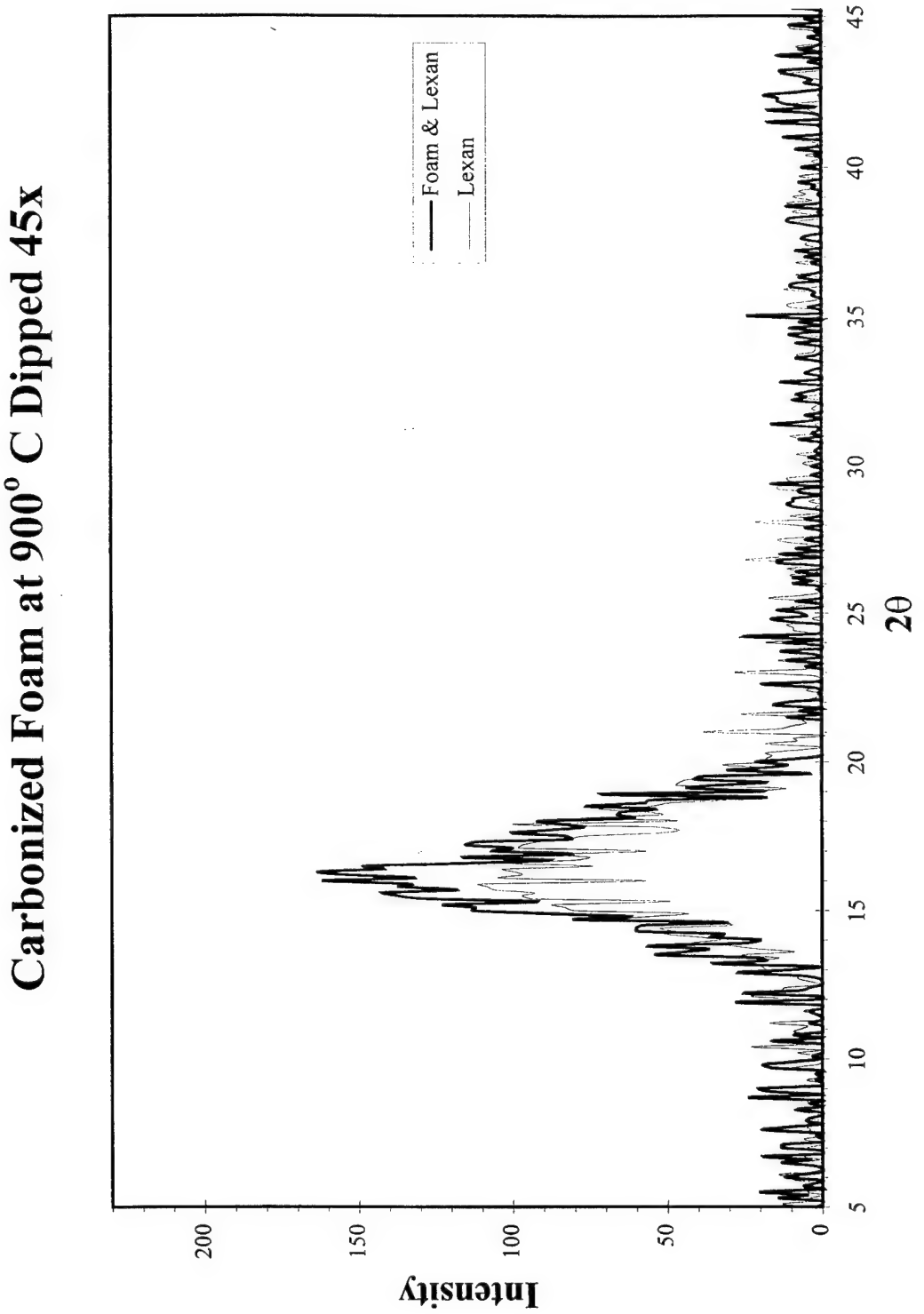

Figure 4-14. X- ray diffraction of Graphitized 45x dipped foam (carbonized 900° C).

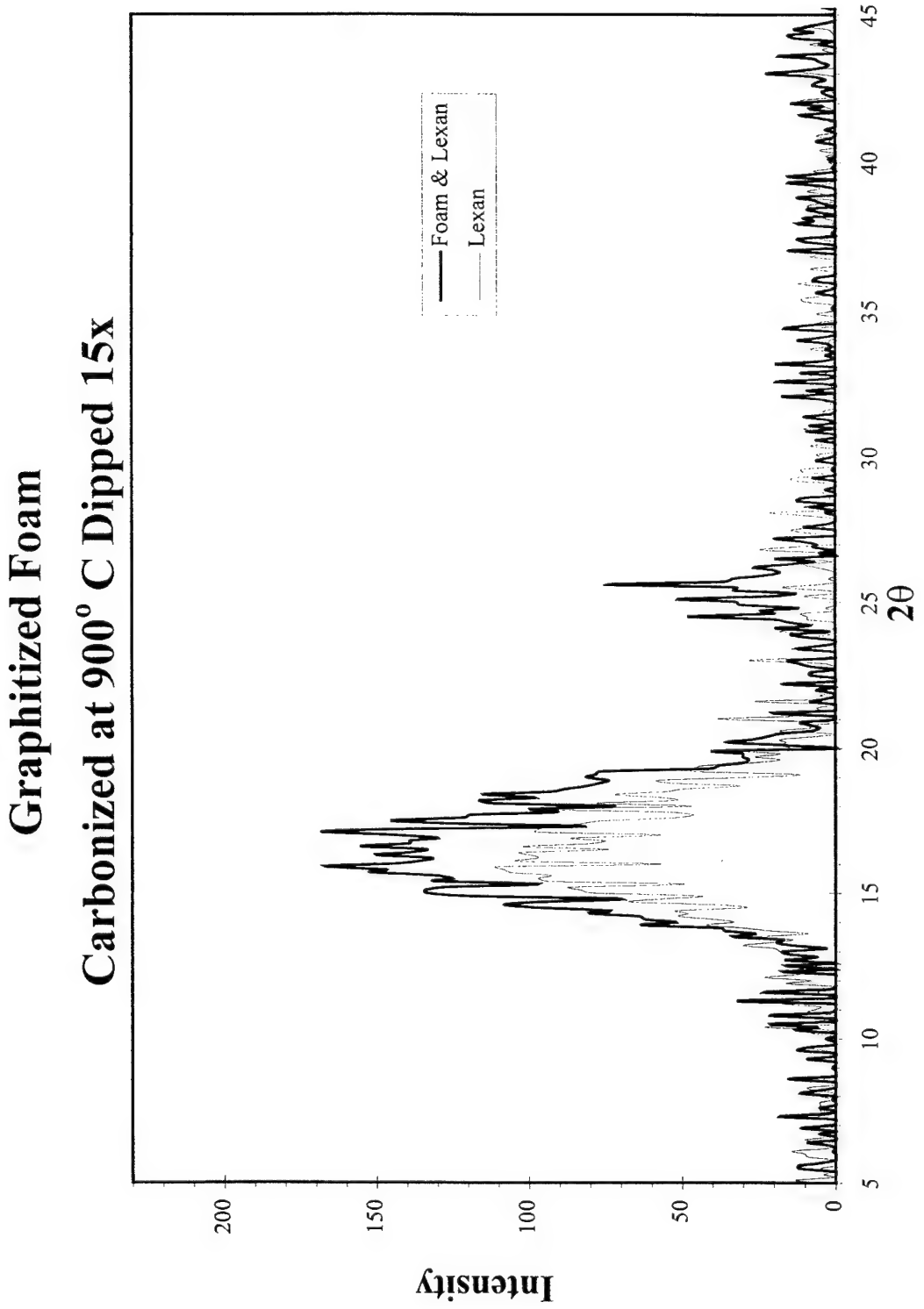

Figure 4-15. X- ray diffraction of 15x dipped foam graphitized (Carbonized at 900° C).

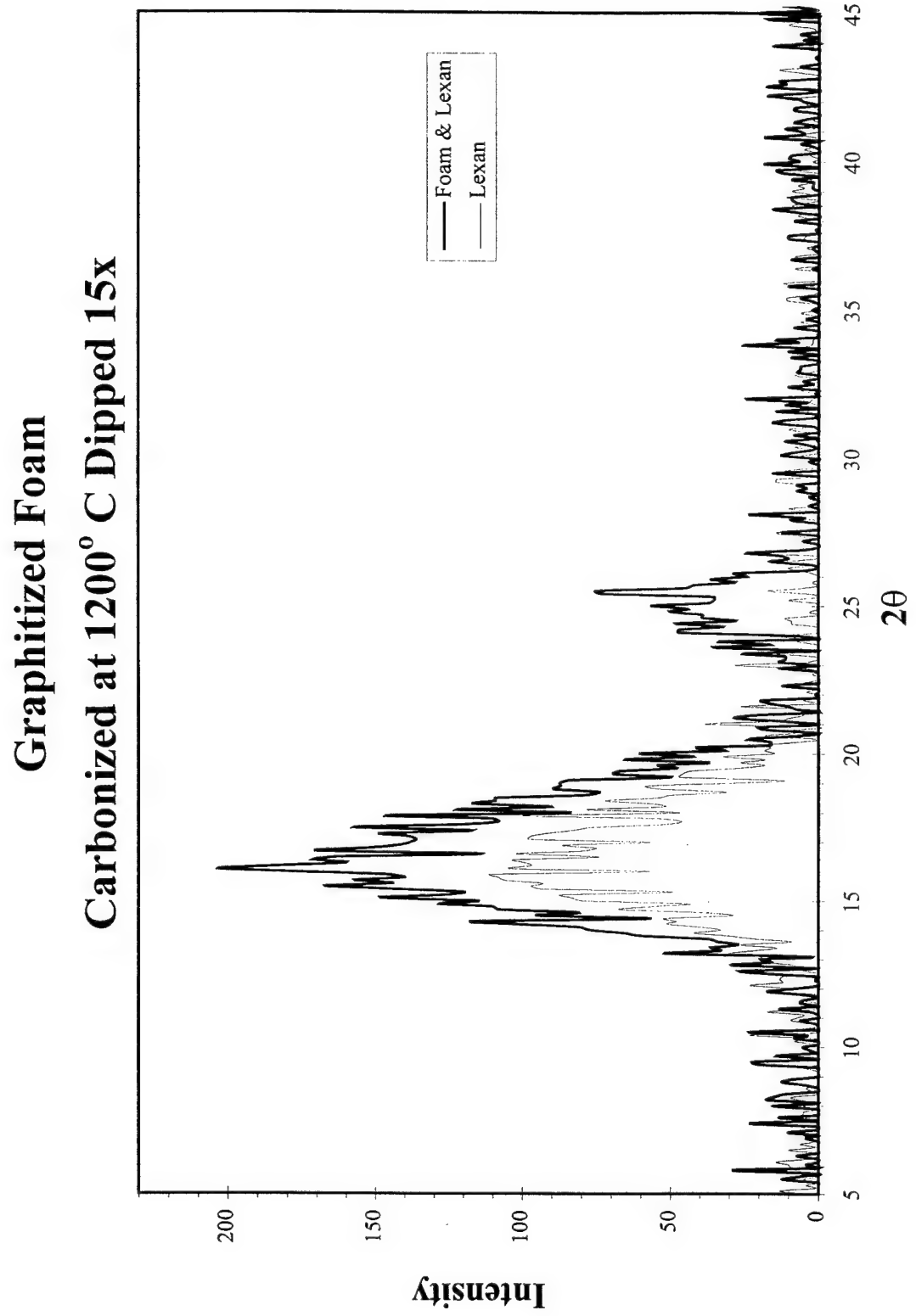

Figure 4-16. X- ray diffraction of 15x dipped foam graphitized (carbonized at 1200° C).

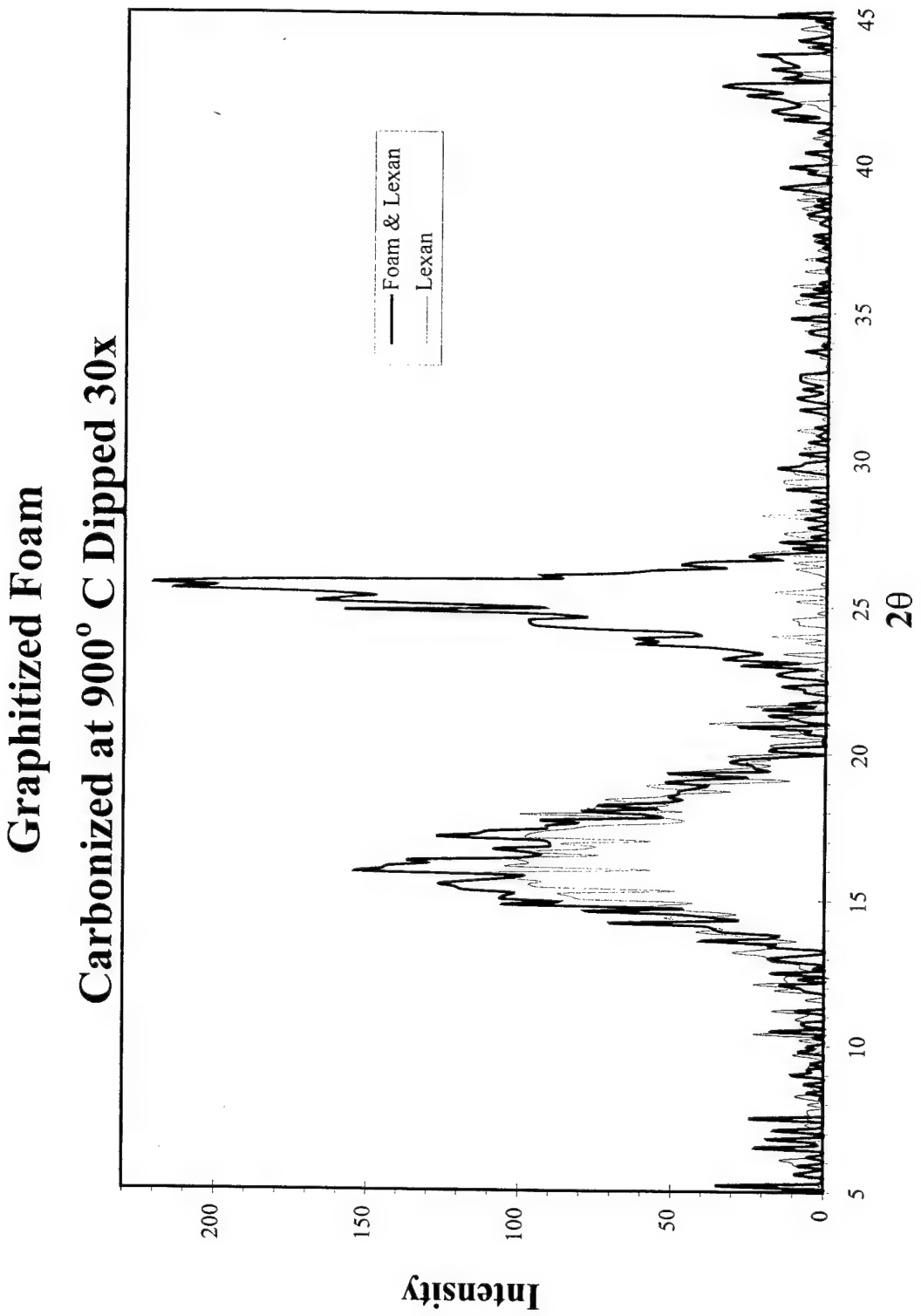

Figure 4-17. X-ray diffraction of 30x dipped foam graphitized (carbonized at 900° C).

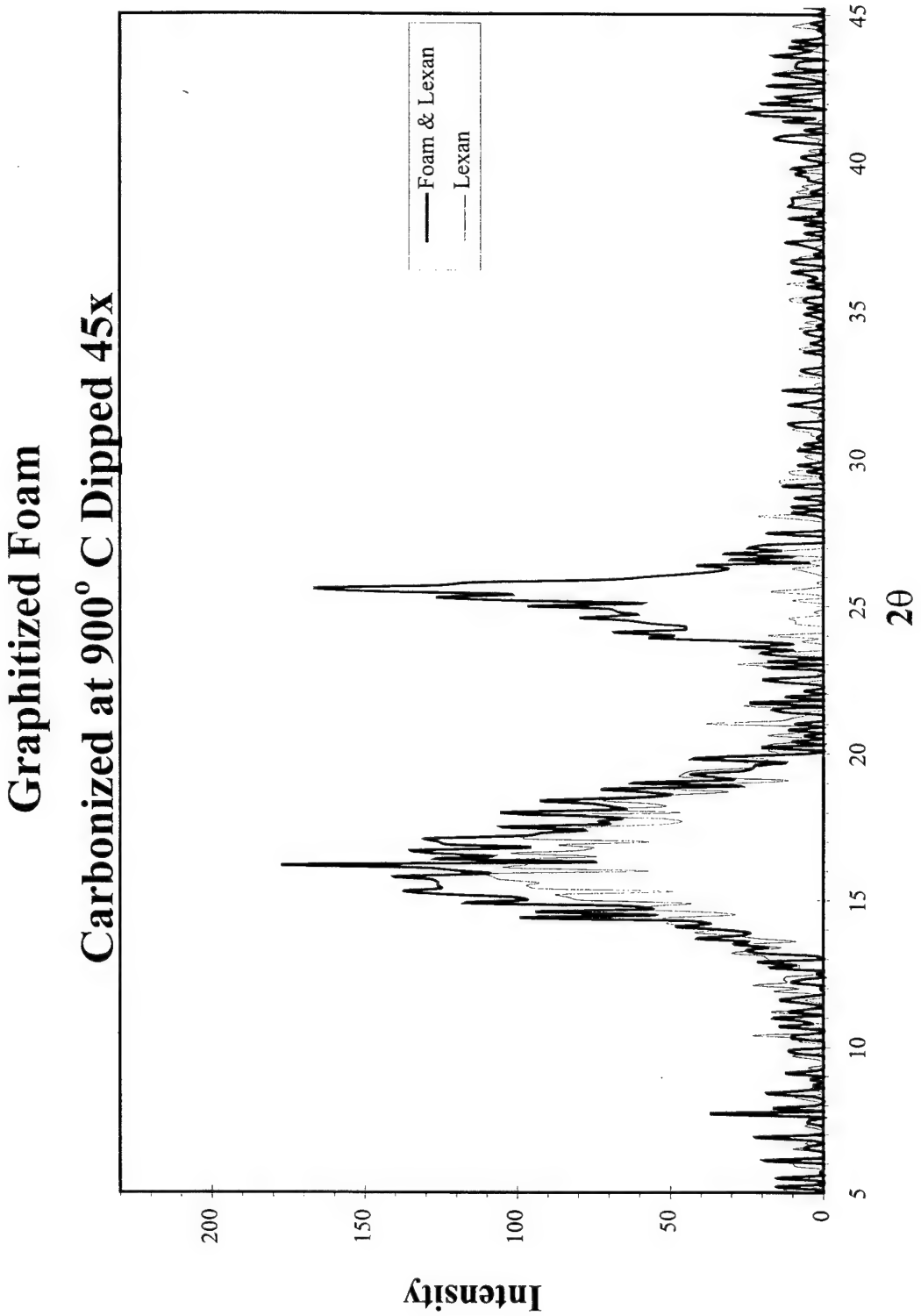

Figure 4-18. X-ray diffraction of 45x dipped foam graphitized (carbonized at 900° C).

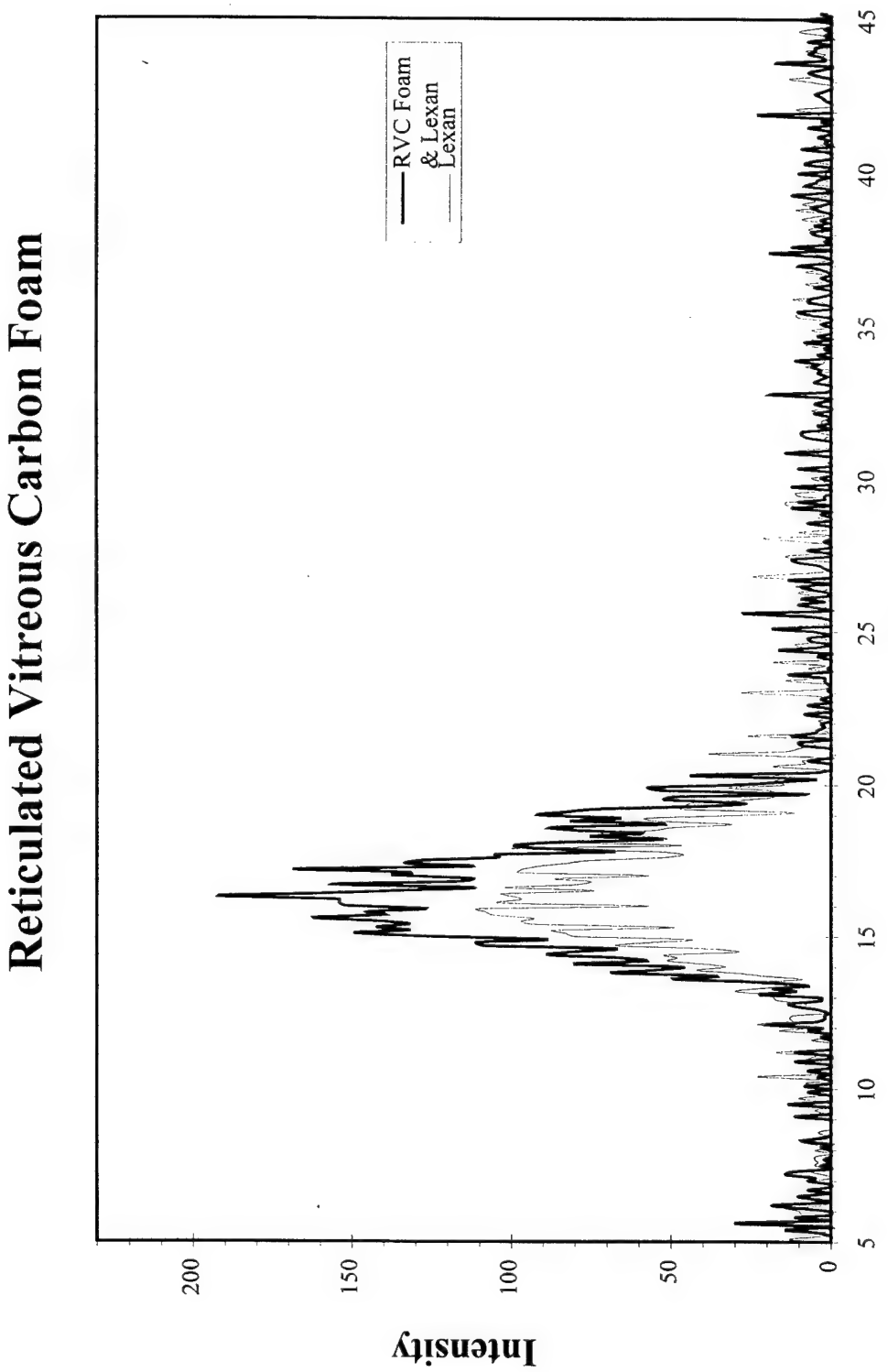

Figure 4-19. X-ray diffraction pattern of RVC foam.

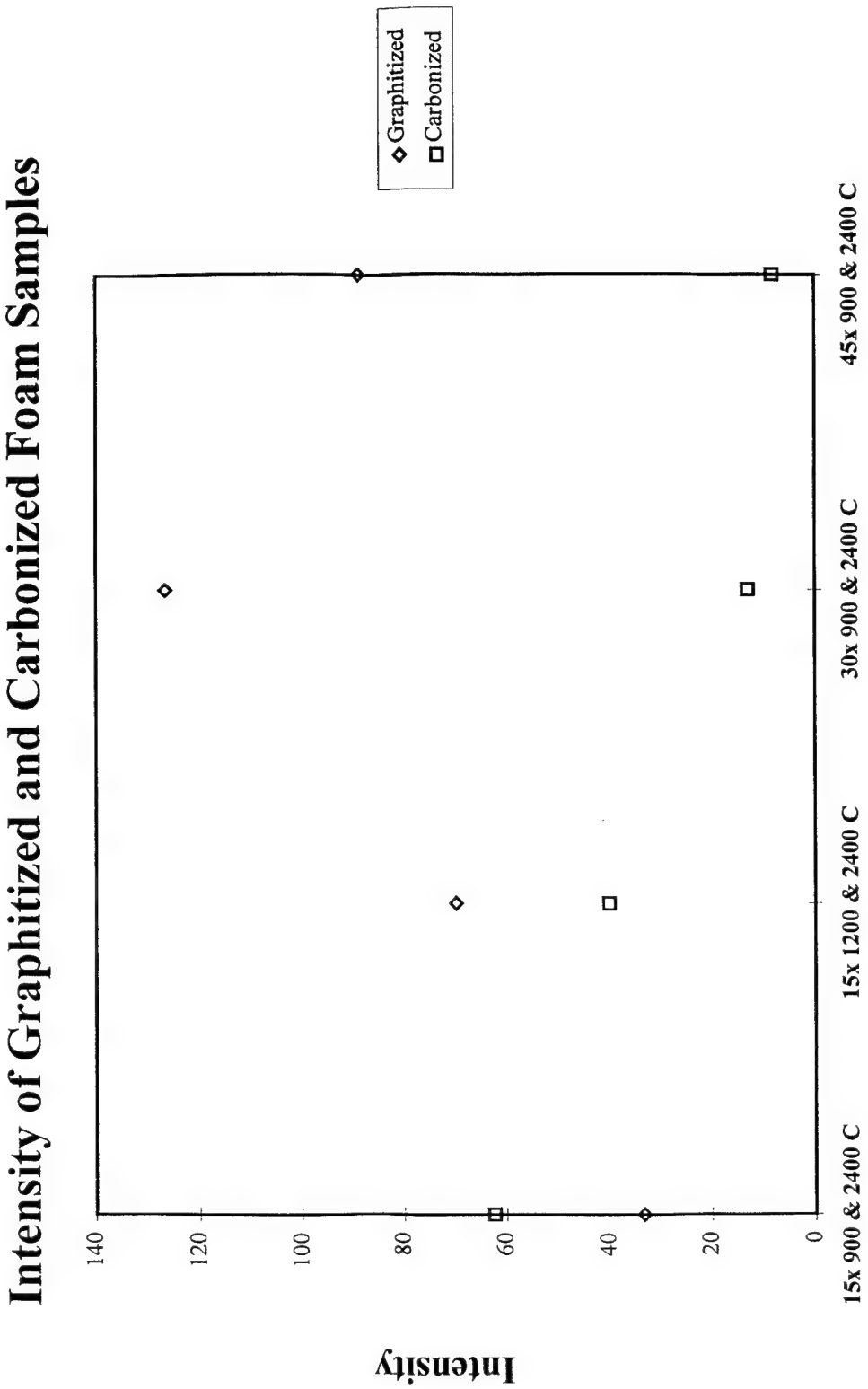

Figure 4-20. Graph of intensities of each graphitized sample.

4.2.2 SCANNING ELECTRON MICROSCOPY

Scanning electron microscopy was done on the foam samples to compare the surface textures and strut cross sections at each stage of preparation.

The polyurethane foam was viewed under an optical microscope. The surface was not smooth along the struts. There were pits and extraneous particles on the surface of the foam. Comparing this to the coated polyurethane foam under the scanning electron microscope shows that coating follows the same contours as the original foam. The mesophase pitch coating was uniform across the entire foam sample (Figure 4-21). The coating texture is relatively smooth along the struts of the foam. There are no gaps in the coating indicating that the pits and valleys of the original polyurethane were filled by the mesophase pitch. The strut cross sections show the triangular shape of the polyurethane foam. The strut shown in Figure 4-21 displays the texture along the cross section of the strut. There are coated particles along the surface of the strut like those seen in Figure 4-22. These pictures give a baseline for a comparison to the foam after each heat treatment stage.

Figure 4-22. SEM of surface texture of dipped foam magnified approx. 150x.

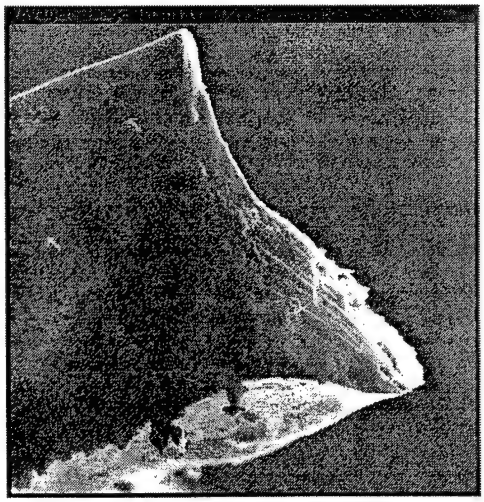

Figure 4-21. SEM of strut cross section of dipped foam magnified approx. 230x.

The surface texture of the oxidized foam (Figure 4-23), as seen under the SEM, shows no apparent difference compared to the dipped foam. The struts still

retain the triangular shape of the polyurethane foam. The texture of the strut cross section is similar to that of the dipped foam.

Figure 4-23. SEM of surface texture of oxidized foam magnified approx. 150x.

Figure 4-24. SEM of strut cross section of oxidized foam magnified approx. 200x.

SEM pictures of the samples after polyurethane burn out were difficult to capture. When the electron beam was directed on the foam, the object of interest would disintegrate. The pictures that were captured are difficult to analyze. They are out of focus, which is due to the movement of the strut as the picture was being captured. The picture of the strut surface appears to be smooth (Figure 4-25), however, this is not an accurate description. It is difficult to examine the surface texture of these foams because they were destroyed each time the SEM was run. The strut cross section was even more difficult to capture. In pointing the beam directly at the strut, it would wither away and actually deform the strut. Pictures of the struts that were effected by the electron beam are not useful in comparing to the other SEM pictures taken. The strut cross section in (Figure 4-26) was taken at a relatively low magnification with the beam not directly on the strut. Again, it is difficult to make any observations as to the texture of the strut. However, the triangular shape of the strut is visible.

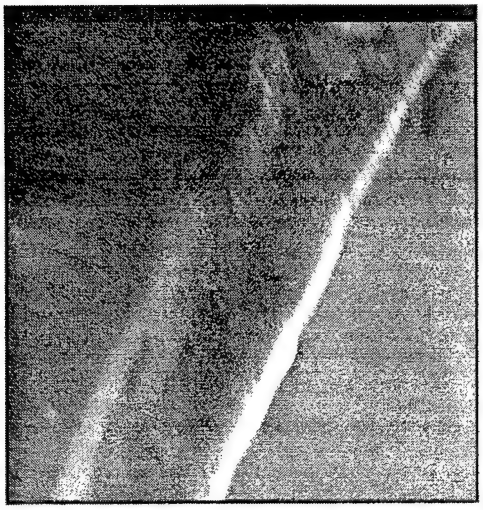

Figure 4-25. SEM of surface texture of foam after polyurethane has been burnt out magnified approx. 150x.

Figure 4-26. SEM of strut cross section of foam after polyurethane has been burnt out magnified approx. 100x.

In the carbonized foam samples, the surface texture looks as if the mesophase pitch coating is layered. The strut surface is smoother than the surface of the dipped and oxidized foams. It is more uniform in that small particles, as seen in the dipped and oxidized foams, have been incorporated into the coating. They may have been removed through the firing process or just blended into the surface. Some of the struts in the carbonized samples were hollow as can be seen in Figure 4-27 and Figure 4-28. The strut cross section of the carbonized foam samples contain the usual triangular shape (Figure 4-29 and Figure 4-30). The end of the strut is relatively smooth, which follows the texture down the surface of the strut. In comparing the surface texture of the carbonized samples with that of the previous samples, it is smoother and more uniform.

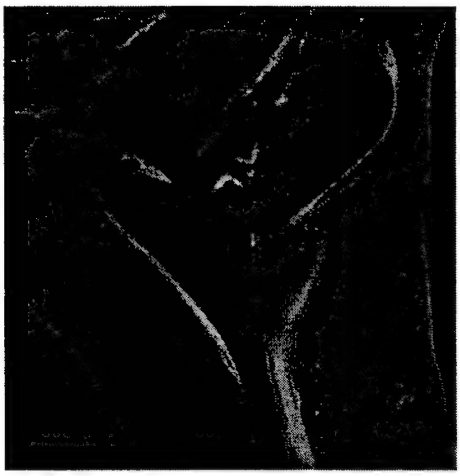

Figure 4-27. SEM of a hollow junction of carbonized foam magnified approx. 140x.

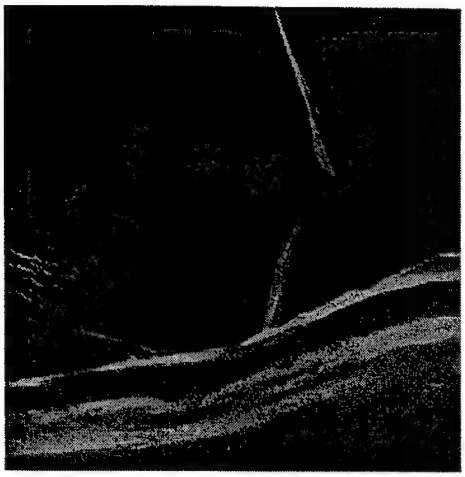

Figure 4-28. SEM of a hollow junction of carbonized foam magnified approx. 200x.

Figure 4-29. SEM of a solid strut of carbonized foam magnified approx. 200x.

Figure 4-30. SEM of a solid strut of carbonized foam magnified approx. 150x.

Scanning electron microscopy was done on each of the four types of graphitized samples. There is a large difference in the surface texture of the graphitized samples as compared to the samples that were dipped, oxidized and carbonized (Figure 4-32). There appears to be two different layers. an outer surface and an inner surface. Figure 4-31 is a blown up picture of Figure 4-32 in which a sheet like layered structure is visible. The struts again possess the triangular shape,

however their size has decreased. They are thinner than the struts previously viewed. Hollow struts were not as frequently found in the graphitized samples. Those that were visible, appeared to be better classified as deep craters than hollow junctions as seen in the carbonized samples.

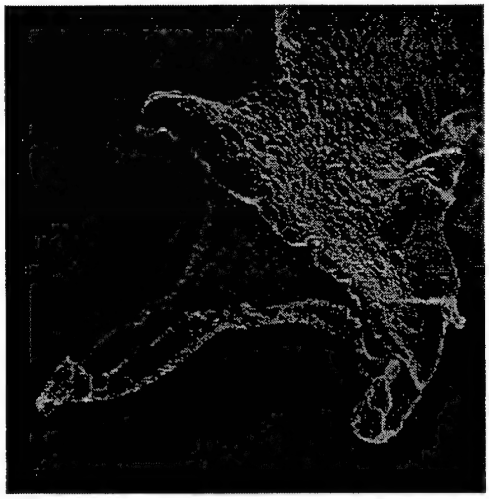

Figure 4-32. SEM of graphitized 15x dipped foam (carbonized at 1200° C) magnified at 170x.

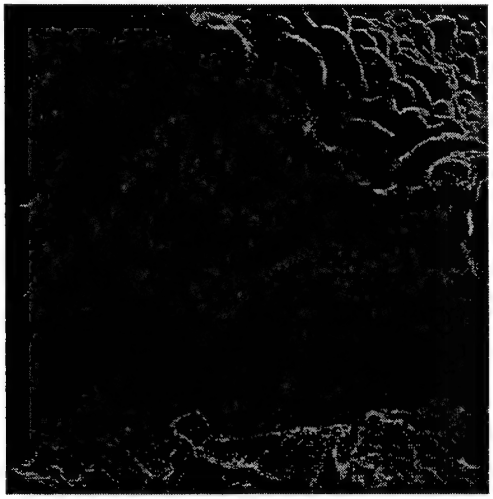

Figure 4-31. SEM of graphitized 15x dipped foam (carbonized at 1200° C) magnified at 650x.

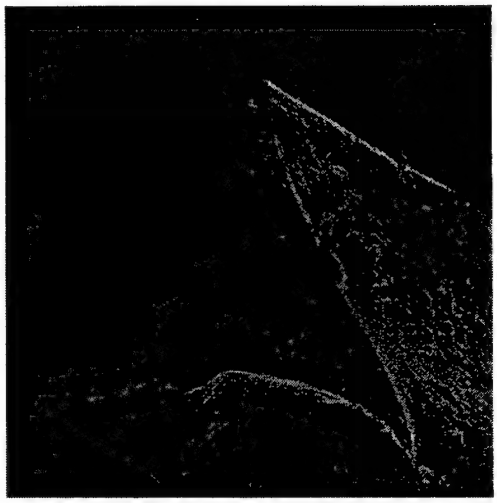

Figure 4-34. SEM of graphitized 30x dipped foam (carbonized at 900° C) magnified approx. 250x.

Figure 4-33. SEM of graphitized 15x dipped foam (carbonized at 900° C) magnified approx. 450x.

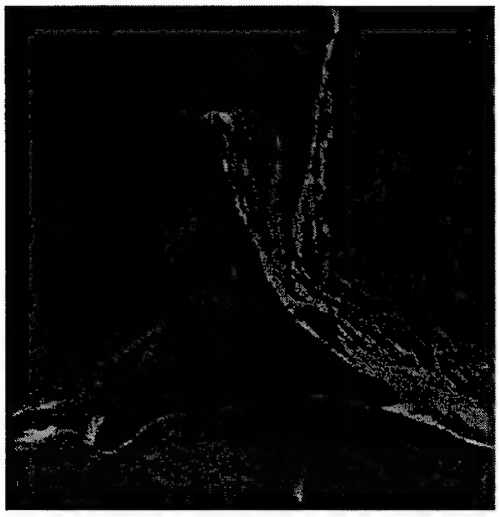

Figure 4-35. SEM of graphitized 45x dipped foam (carbonized at 900° C) magnified approx. 170x.

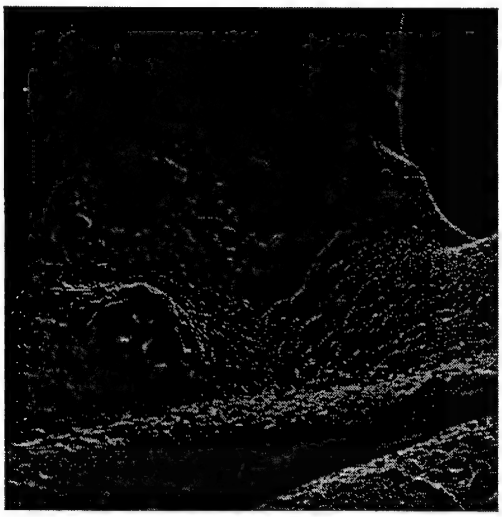

Figure 4-36. SEM of graphitized 45x dipped foam (carbonized at 900° C) magnified approx. 170x.

Each of the four samples viewed under the SEM contain unique surface characteristics. Both of the graphitized 15x dipped samples contain a rougher surface texture compared to the 30x and 45x dipped samples. The texture of all carbonized samples is smoother than the graphitized foams. A comparison of the graphitized foam with vitreous carbon (Figure 4-37) shows that the surface texture is more defined and course. The vitreous carbon is very smooth and contains no defects, making it difficult to focus on. The graphitic foam has the complete opposite in surface texture. Based on the surface texture comparison, it can be concluded that the foam produced using mesophase pitch is not a vitreous carbon.

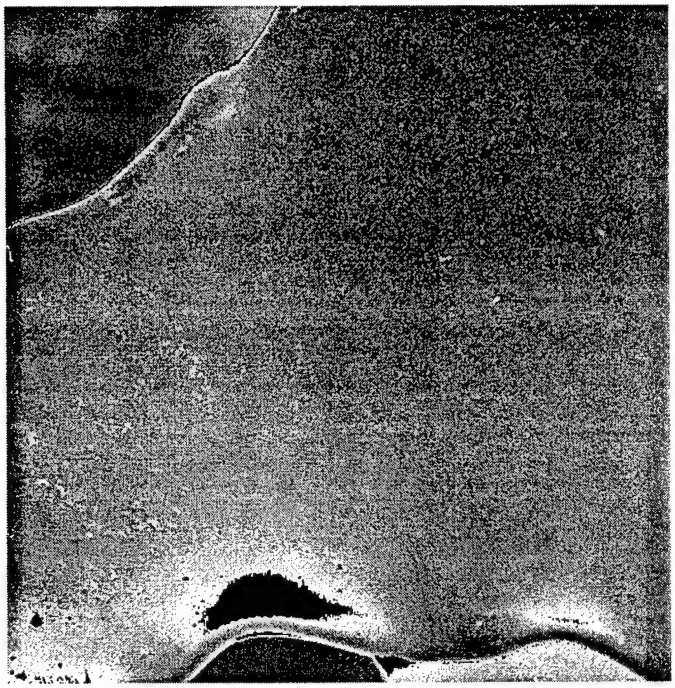

Figure 4-37. SEM of reticulated vitreous carbon foam magnified approximately 200x.

The final reticulated graphitic foam, as seen under SEM, is seen in Figure 4-38. The diameter of the bubbles are approximately 2 - 3 mm, and the thickness of the struts varies between 0.2 - 0.4 mm. This translates to about an 18 - 20 ppi foam density. The original polyurethane foam was 10 ppi. Therefore the foam shrinkage is about one half of the starting size.

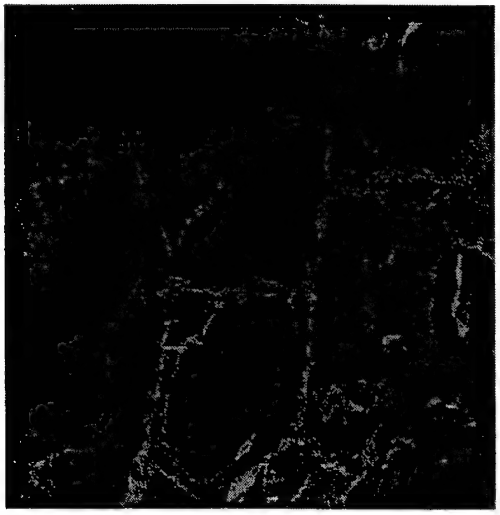

Figure 4-38. SEM of sample C magnified approx. 15x.

4.3 CONCLUSIONS AND FUTURE WORK

The foam produced using polyurethane foam as a fugitive phase can be used to create a graphitic foam. The application of coating a flexible polyurethane foam for a fugitive phase in producing graphitic foam gives the ability to choose the cell density for a particular application.

The samples dipped 30x reveal slightly higher intensities than the other samples run under x-ray diffraction. Based on the mass loss data and the x-ray diffraction analysis, the 30x dipped foam samples carbonized at 900° C and then graphitized at 2400° C may prove to be a useful technique for producing the graphitic foam. The change in mass is very similar to the other samples run, however, preliminary analysis shows that more graphite may be present in the samples dipped 30x.

The x-ray diffraction analysis shows that graphite is present in the foam. The scanning electron microscopy performed further reinforces the x-ray analysis done on the foam. However, it is not known the amount of graphite present and this is difficult to conclude from the x-ray diffraction data. All that can be deduced from the

data is that graphite exists. The samples dipped 45x and 30x would expect to contain more graphite than the samples dipped only 15x.

Further x-ray diffraction analysis should be completed to characterize the crystalline size and amount of the graphite present in the struts. This can be done by adding a known amount pure graphite to a known amount of the sample and running the samples through the region where the (002) peak exists in the graphite standard. The intensity is proportional to the amount added in the material and thus it can be determined the amount of graphite in the foam. As the percentage of graphite is increased in the sample, the dominant peak will become more pronounced, which is representative of graphite in the sample.

It would be interesting to graphitize the foam created using blowing agents and analyze it for evidence of graphite. This might give some insight as to how the polyurethane affects the mesophase pitch through each heat treatment. A comparison of the x-ray diffraction pattern of the two foams produced may give some indication of the formation of graphite in the polyurethane coated foam. The pitch blown foam could be used as a control, since it is relatively pure in pitch.

Characterization of the mesophase pitch coating and its interaction with the polyurethane is necessary to determine what role the polyurethane plays in the process. Questions that should be addressed are: does the polyurethane aid or hinder graphite formation in the mesophase pitch, does the solvent play a role in this process other than dissolving the mesophase pitch, does the amount of mesophase pitch effect the amount of graphite present in the sample.

5. SUMMARY

Two different methods of producing graphitic carbon foams from mesophase pitch were presented in this thesis. The first consisted of two variations of the blowing agent method, and the second utilized a pre-existing foam as a fugitive phase.

The use of blowing agents was successful in producing a foam, however the morphology was not desirable. The direct blowing method produced a foam with a fine cell structure, with a bubble size of approximately 0.4 mm in size. Bubbles of 1 mm in size could also be produced using this method, however the structure was closed cell. The open cell morphology could not be achieved in either of the blowing methods. Reblowing the foam was unsuccessful. The original structure was lost either by collapse or by shattering.

An open celled foam was created using polyurethane as a fugitive phase. The use of polyurethane foam as a fugitive phase allows control over the cell morphology. Upon heat treatment of the foam, a graphitic foam was created. The graphite was detected using x-ray diffraction. The final porosity of the foam is estimated to be between 18 and 20 ppi.

6. REFERENCES

1 G. Murray, Feasibility Studies for Novel Applications of Cellular Ceramic Materials, M.S. Thesis at Clarkson University, (1995).

2 Ultramet, 12173 Montague Street, Pacoima, California 91331.

3 Cheremisinoff, P.N., and Ellerbusch, F., Carbon Adsorption Handbook, Ann Arbor Science Publishers Inc. (1988).

4 Hall, R.B. and Hager, J.W., "Graphitic Foams As Potential Structural Materials", 21st Biennial Conference on Carbon, Extended Abstracts, American Carbon Society, 102-103, 1993.

5 Gibson, L.J. and Ashby, M.F., Cellular Solids Structure and Properties, Pergamon Press, (1988).

6 Ashby, M.F., *Acta Metall.*, **37**, 1273-1293, (1989).

7 Mehta, R., Anderson, D.P., Hager, J.W., and Thorp, K.E.G., "Graphitic Carbon Foams: Processing and Characterization", *21st Biennial Conference on Carbon, Extended Abstracts, American Carbon Society*, 104-105, 1993.

8 Frisch, K.C., and Saunders, J.H., Handbook of Plastic Foams, Marcel Dekker, Inc., (1972).

9 Arnold, C. Jr., Aubert, J.H., Clough, R.L., Rand, P.B. and Sylwester, A.P., US Pat no. 4832881, (1989).

10 Dutta, D. and Hill, C.S. "Aligned Graphitic Carbon Foams from Mesophase Pitch" IR (1994).

11 R.W. Pekala, and R.W. Hopper, Low Density Microcellular Carbon Foams, *Journal of Materials Science*, **22**, 1840-1844, (1987).

12 Colton, J.S., and Suh, N.P., "Nucleation of Microcellular Foam: Theory and Practice", *Polymer Engineering and Science*, **27**, 500 - 503, (1987).

13 Colton, J.S., and Suh, N.P., "Nucleation of Microcellular Thermoplastic Foam with Additives: Part I: Theoretical Considerations", *Polymer Engineering and Science*, **27**, 485 - 492, (1987).

14 Colton, J.S., and Suh, N.P., "Nucleation of Microcellular Thermoplastic Foam with Additives: Theoretical Considerations: Part II: Experimental Results and Discussion", *Polymer Engineering and Science*, **27**, 493 - 500, (1987).

15 J.H. Aubert, R.L. Clough, *Polymer*, (1986).

16 Coudeville, A., Eyharts, P., Perrine, J.P., Rey, L., and Rouillard, R.J., *Vac. Sci. Technol.*, **18**, 1227, (1981).

17 Young, A.T., Moreno, D.K., and Marsters, R.G., *Vac. Sci. Technol.*, **20**, 1094, (1982).

18 J.H. Aubert, A.P. Sylwester, "Microcellular Foams? For What?" *CHEMTECH*, **21**, 234, (1991).

19 Aubert, J.H., Sylwester, A.P., "Morphological Characterization of Microcellular Carbon Foams", *J. Materials Science*, **26**, 5741,(1991).

20 ERG 900 Stanford Ave, Oakland, California 94608.

21 Gerald, J.D., Pennock, G. M. and Taylor, G. H., *Carbon* **29**, 140 (1991).

22 Polymeric Carbons - Carbon Fiber, Glass and Char

23 G.C. Merriam, Webster's New Collegiate Dictionary, Springfield, MA, (1956).

24 Toshima, H., Mochida, I., Korai, Y., Murakami, K., and Hino, T., "Characterization of Mesophase Pitch Through Structural Analyses of Insoluble Fractions Solubilized by Eiels-Alder Reaction",

25 Savage, G., Carbon - Carbon Composites, Chapman & Hall, (1993).

26 Singer, L.S., "Mesophase in Carboneous Pitches", *Faraday Discuss. Chem. Soc.*, **79**, 265-272, (1985).

27 Anderson, D.P., Wapner, P.G., and Curliss, D.B., *Mat. Res. Soc. Symp. Proc.*, **270**, 59, (1992).

28 Mochida, I., Ling, L., and Korai, Y., *J. Material Science*, **29**, 3056, (1994).

29 Yoon, S.H., Korai, Y., Mochida, I.., and Kato, I., *Carbon*, **32**, 273, (1994).

30 ōtani, S., "Carbonaceous Mesophase and Carbon Fibers", *Mol. Cryst. Liq. Cryst.*, **63**, 249, (1981).

31 Murrell, J.N., and Jenkins, A.D., Properties of Liquid Crystals, John Wiley & Sons, (1994).

32 Peebles, L.H., Carbon Fibers Formation, Structure, and Properties, CRC Press, (1994).

33 Correspondence with Mitsubishi Gas Chemical Company, Inc. Japan.

34 Roche, E.J., Lavin, J.G., and Parrish, R.G., *Carbon*, **26**, 911, (1988).

35 Baldwin, D.F., and Suh, N.P., *ANTEC*, 1503, (1992).

36 Drbohlav, J., and Stevenson, W.T.K., "The Oxidative Stabilization and Carbonization of a Synthetic Mesophase Pitch, Part I: The Oxidative Stabilization Process", Wichita State, 1994.

37 Goel, S.K. and Beckman, E.J., *AIChE Journal*, **41**, *2*, 357 (1995).

38 Kumar, V. and Weller, J.E., *ANTEC*, 1402 (1991).

39 Crank, J., Mathematics of Diffusion Handbook, Oxford at The Clarendon Press, (1967).

40 Kumar, V. Weller, J.E. and Montecillo, R. Microcellular PVC, *ANTEC*, 1452-1456, (1992).

41 Kumar, V. and Weller, J.E. "Creating an Integral, Unfoamed Skin on Microcellular Foams", *ANTEC*, 1508-1512, (1992).

42 Reid, R.C., Prausnitz, J.M., and Poling, B.E., The Properties of Gases and Liquids, 4th Edition, McGraw-Hill Book Co., (1986).

43 Ramesh, N.S., Dontula, N., Rasmussen, D. and Campbell, G.A., *ANTEC*, 1292, (1991).

44 Amon, M. and Denson, C.D., *Polymer Engineering and Science*, **24**, 1027 (1984).

45 Rosner, D.E. and Epstein, M., *Chemical Engineering Science*, **27**, 69 (1972).

46 Barrett, C.R., Nix, W.D., and Tetleman, A.S., **Principles of Engineering Materials**,

Prentice-Hall, Inc. (1973).

47 Jenkins, G.M., Kawamura, K., Polymeric Carbons - Carbon Fiber, Glass and Char, Cambridge University Press, (1976).